http://www.TheoryOfEverything.org

Mapping the fourfold H_4 600-cells emerging from E_8: A mathematical and visual study

J Gregory Moxness*
TheoryOfEverything.org
(Dated: August 10, 2018)

It is widely known that the E_8 polytope can be folded into two Golden Ratio (Φ) scaled copies of the 4 dimensional (4D) 120 vertex 720 edge H_4 600-cell. While folding an 8D object into a 4D one is done by applying the dot product of each vertex to a 4×8 folding matrix, we use an 8×8 rotation matrix to produce four 4D copies of H_4 600-cells, with the original two left side Φ scaled 4D copies related to the two right side 4D copies in a very specific way. This paper will describe and visualize in detail the specific symmetry relationships which emerge from that rotation of E_8 and the emergent fourfold copies of H_4. It will also introduce a projection basis using the Icosahedron found within the 8x8 rotation matrix. It will complete the detail for constructing E_8 from the 3D Platonic solids, Icosians, and the 4D H_4 600-cell. Eight pairs of Φ scaled concentric Platonic solids are identified directly using the sorted and grouped 3D projected vertex norms present within E_8. Finally, we will show the relationship of the Beordijk-Coxeter Tetrahelix emerging from the Petrie projection's concentric rings of 30 vertices of the H_4 600-cells.

PACS numbers: 02.20.-a, 02.10.Yn
Keywords: Coxeter groups, root systems, E8

I. INTRODUCTION

Fig. 1 is the Petrie projection of the largest of the exceptional simple Lie algebras, groups and lattices called E_8. It has 240 vertices and 6720 edges of 8D length $\sqrt{2}$. Interestingly, E_8 has been shown to fold to the 4D Polychora of H_4 (a.k.a. the 120 vertex 720 edge 600-cell) and a scaled copy $H_4\Phi[1][2]$, where $\Phi = \frac{1}{2}\left(1+\sqrt{5}\right) = 1.618...$ is the big Golden Ratio and $\varphi = \frac{1}{2}\left(\sqrt{5}-1\right) = 1/\Phi = \Phi - 1 = 0.618...$ is the small Golden Ratio. Fig. 2 shows the folding orientation of E_8 Dynkin diagram above the H_4 Coxeter-Dynkin diagram.

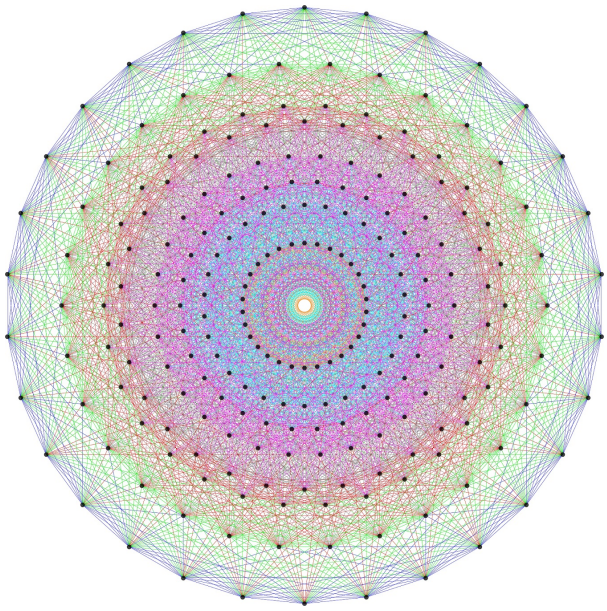

*URL: http://www.TheoryOfEverything.org/TOE/JGM; mailto:jgmoxness@TheoryOfEverything.org

FIG. 1: E_8 Petrie projection

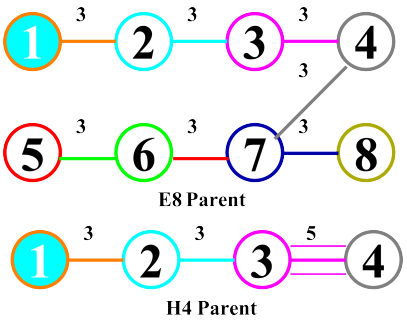

FIG. 2: a) E_8 Dynkin diagram in folding orientation b) The associated Coxeter-Dynkin diagrams H_4

There are several choices for the form of E_8, whether it be complex or split real (even or odd). For the purposes of this work, the form selected is split real even (SRE). While the basic topology of the E_8 Dynkin diagram is unique, it has 8!=40320 permutations of node ordering. The node order used here is given in Fig. 2a. The 240 specific E_8 group vertex values are determined from the simple roots matrix $\mathrm{E8_{srm}}$ shown in (1) by using the weights of the 120 positive (and 120 negative) roots generated from the Lie algebra applied to the Cartan matrix, calculated here in (2). It can also be derived directly from the structure and node order of the E_8 Dynkin diagram.

$$\mathrm{E8_{srm}} = \begin{pmatrix} 1 & -1 & 0 & 0 & 0 & 0 & 0 & 0 \\ 0 & 1 & -1 & 0 & 0 & 0 & 0 & 0 \\ 0 & 0 & 1 & -1 & 0 & 0 & 0 & 0 \\ 0 & 0 & 0 & 1 & -1 & 0 & 0 & 0 \\ -\frac{1}{2} & -\frac{1}{2} & -\frac{1}{2} & -\frac{1}{2} & -\frac{1}{2} & -\frac{1}{2} & -\frac{1}{2} & -\frac{1}{2} \\ 0 & 0 & 0 & 0 & 0 & 1 & 1 & 0 \\ 0 & 0 & 0 & 0 & 1 & -1 & 0 & 0 \\ 0 & 0 & 0 & 0 & 0 & 1 & -1 & 0 \end{pmatrix} \tag{1}$$

$$\mathrm{E8_{Cartan}} = \mathrm{E8_{srm}}.\mathrm{E8_{srm}^T} \tag{2}$$

Rather than folding by taking the dot product of a 4×8 folding matrix against each of the 240 vertices of the SRE E_8, we rotate it using the 8×8 square rotation matrix. Unlike folding to 4D, the rotation preserves the integrity of E_8, including the 28680 edges of the complete graph, without losing the ability to identify the individual and combined 4D H_4 and $H_4\Phi$ edges. The specific matrix for performing the rotation of the SRE E_8 group of vertices was shown[3] to be that of (3). Notice that $\mathrm{H4_{rot}} = \mathrm{H4_{rot}^T}$ such that it is symmetric with a quaternion-octonion Cayley-Dickson-like structure. Only the first 4 rows are needed for folding E_8 to H_4. The result is not two, but four copies of H_4 600-cell with the left (L) 4 dimensions associated with the two scaled copies (H_4 and $H_4\Phi$) and the right (R) 4 dimensions associated with another two copies (H_4 and $H_4\Phi$).

$$\mathrm{H4_{rot}} = \begin{pmatrix} \Phi & 0 & 0 & 0 & \varphi^2 & 0 & 0 & 0 \\ 0 & -\varphi & 1 & 0 & 0 & \varphi & 1 & 0 \\ 0 & 1 & 0 & -\varphi & 0 & 1 & 0 & \varphi \\ 0 & 0 & -\varphi & 1 & 0 & 0 & \varphi & 1 \\ \varphi^2 & 0 & 0 & 0 & \Phi & 0 & 0 & 0 \\ 0 & \varphi & 1 & 0 & 0 & -\varphi & 1 & 0 \\ 0 & 1 & 0 & \varphi & 0 & 1 & 0 & -\varphi \\ 0 & 0 & \varphi & 1 & 0 & 0 & -\varphi & 1 \end{pmatrix} \tag{3}$$

A. Deconstructing the H_4 600-cell

Each copy of the 600-cell is made up 120 vertices shown in Fig. 3 in E_8 Petrie projection (or two Φ scaled copies of the Van Oss projection when used in conjunction with 600-cells), with 24 of the 120 vertices making up the self-dual

24-cell. The 24-cell is in turn made up of the 16 vertices of the 8-cell a.k.a. Tesseract, 4-cube, 5-DemiCube or BC_5 (Fig. 3a off-axis blue dots) and the 8 vertices of the 16-cell a.k.a. 4D Cross Polytope or 4-Orthoplex (Fig. 3a on-axis red dots), each of these being the dual of the other. The other 96 vertices of the 600-cell are those of the Snub 24-cell, which can be visualized in 2D by rotating the 24-cell four times in increments of $\pi/5$ (as shown in Fig. 3b red, green, blue, yellow) or projected to 3D (as shown in Fig. 4).

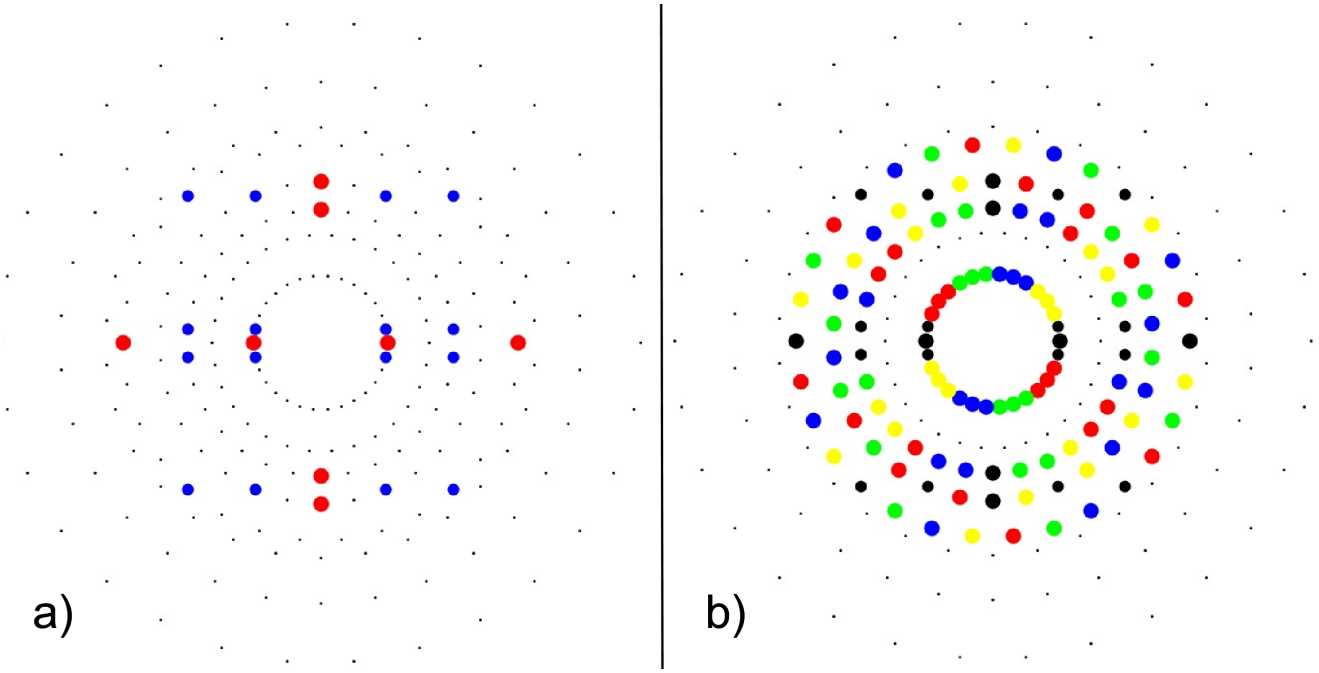

FIG. 3: a) 24-cell highlighting the 16-cell (red on-axis vertices) and 8-cell (blue off-axis vertices), b) Snub 24-cell highlighting four $\pi/5$ rotations of the 24-cell (black) in red, green, blue, yellow

In applying $\mathrm{H4_{rot}}$ to each vertex of E_8, the 4 quadrants of (3) naturally produce 4D H_4 L=R symmetry from E_8 vertices that have L=R symmetry. The 16 L=R E_8 $\frac{1}{2}$ integer vertices are shown to be the 16 vertices of the 8-cellΦ permutations of $\{\pm1, \pm1, \pm1, \pm1\}$. Interestingly, the 16 L=-R $\frac{1}{2}$ integer E_8 vertices give the vertices of the 8-cell permutations of $\{\pm\varphi, \pm\varphi, \pm\varphi, \pm\varphi\}$. There are 8 integer E_8 vertices that have L=R symmetry and 8 that have L=-R. These rotate into the two scaled copies of the 16-cellΦ permutations of $\{\pm2, 0, 0, 0\}$ and 16-cell permutations of $\{\pm2\varphi, 0, 0, 0\}$ within $H_4\Phi$ and H_4 respectively. A full list of E_8 and H_4 rotated vertices is shown in Appendix A.

It isn't immediately obvious that there are other symmetries involved in the remaining 2*96=192 vertices of the L/R 600-cells, namely those of the scaled copies Snub 24-cell permutations of $\{0, \pm1, \pm\varphi, \pm\varphi^2\}$ and Snub 24-cellΦ permutations of $\{0, \pm1, \mp\varphi, \pm\Phi\}$. It is clear from Appendix A that this $L \leftrightarrow R$ relationship from E_8 is not L=R or L=-R. Careful analysis of the 28680 edges in the complete graph of the rotated E_8 shows otherwise. This is discussed in more detail in Section II and III.

B. Projecting E_8 and H_4

Projection of E_8 to 2D (or 3D) requires 2 (or 3) basis vectors $\{X, Y, Z\}$. We start with those in (4), which are simply the two 2D Petrie projection basis vectors of the 600-cell (a.k.a. the Van Oss projection) as shown in Fig. 3, with a 3rd (z) basis vector added for the 3D projection. Notice the 8D basis vectors with zero in the last 4 columns (or dimensions), highlighting the fact that E_8 projection is based on a 4D H_4 construct.

$$\begin{array}{lccccc} \mathrm{x}=\{ & 0, & \Phi 2\mathrm{Sin}\frac{2\pi}{15}, & 2\mathrm{Sin}\frac{2\pi}{15}, & 0, & 0,0,0,0\} \\ \mathrm{y}=\{ & 1, & 0, & 0, & \Phi 2\mathrm{Sin}\frac{2\pi}{30}, & 0,0,0,0\} \\ \mathrm{z}=\{ & -\Phi 2\mathrm{Sin}\frac{2\pi}{30}, & 0, & 0, & 1, & 0,0,0,0\} \end{array} \tag{4}$$

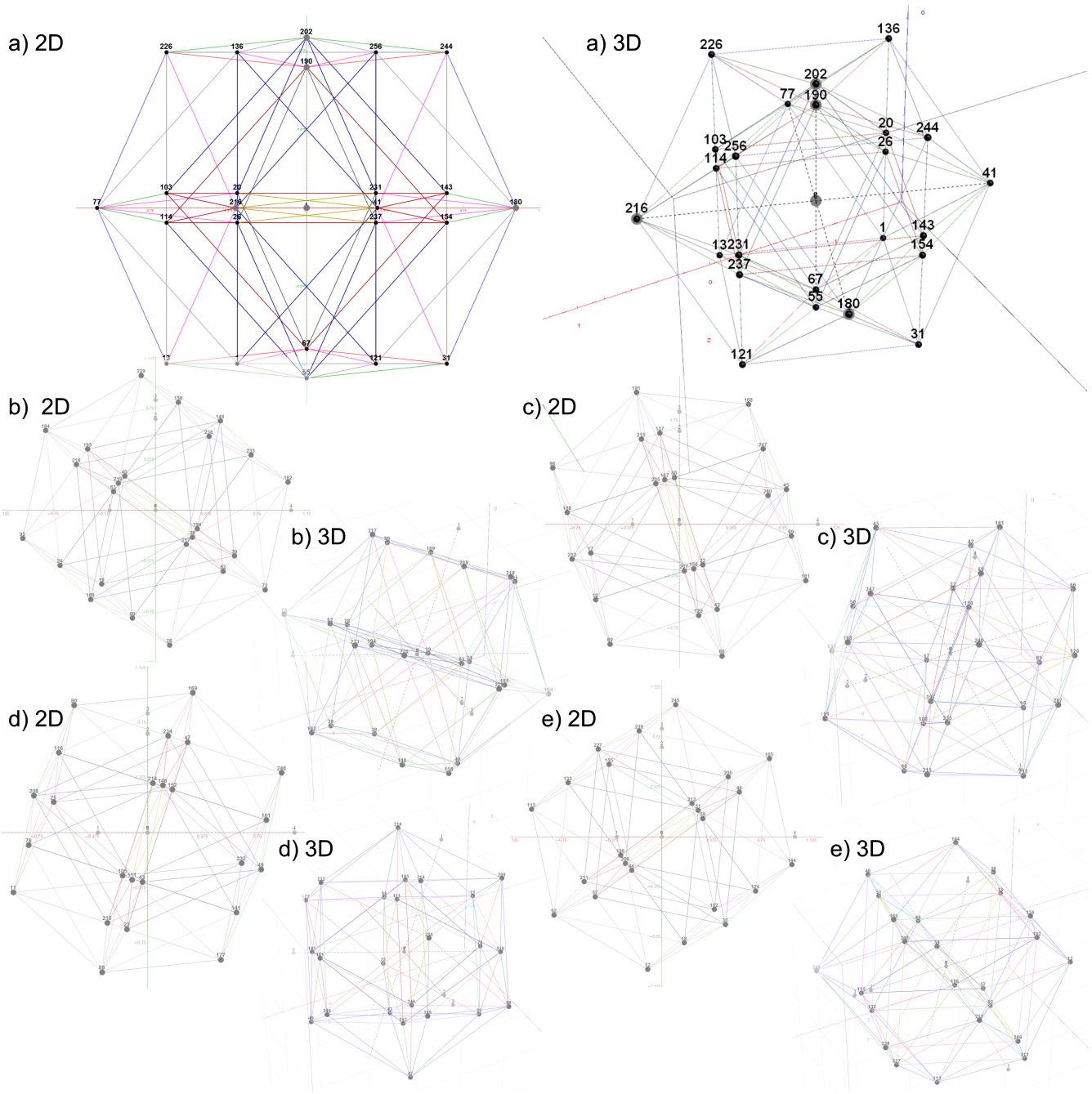

FIG. 4: The 5 24-cell decomposition of one 600-cell, each with 2D and 3D vertex numbered projections including edges; a) 24-cell, b-e) Snub 24-cells from four $\pi/5$ rotations of the 24-cell in a)

$$\begin{array}{lllllllll} \text{X}=\{ & 0, & -.068, & .168, & -.329, & 0, & .476, & .168, & .329\} \\ \text{Y}=\{ & .655, & 0, & -.137, & .084, & -.155, & 0, & .137, & .084\} \\ \text{Z}=\{ & -.221, & 0, & -.405, & .250, & .052, & 0, & .405, & .250\} \end{array} = \text{H4}_{\text{rot}}^{-1}.\{x, y, z\} \tag{5}$$

Fig. 5 in 3D shows the same projection shown in Fig. 1 in 2D by adding the Z basis vector to the projection. The result is that one face (or 2 of 6 cubic faces, which are the same), it projects E_8 to its 2D Petrie projection and on another face pair it projects to the 2D orthonormal view of the 600-cell. The third face pair is a rotation between the other two pairs of faces. While the concentric structure of the scaled H_4 polytopes is visible by noticing the green interior edges, a more dramatic 3D visualization is described in the section IV.

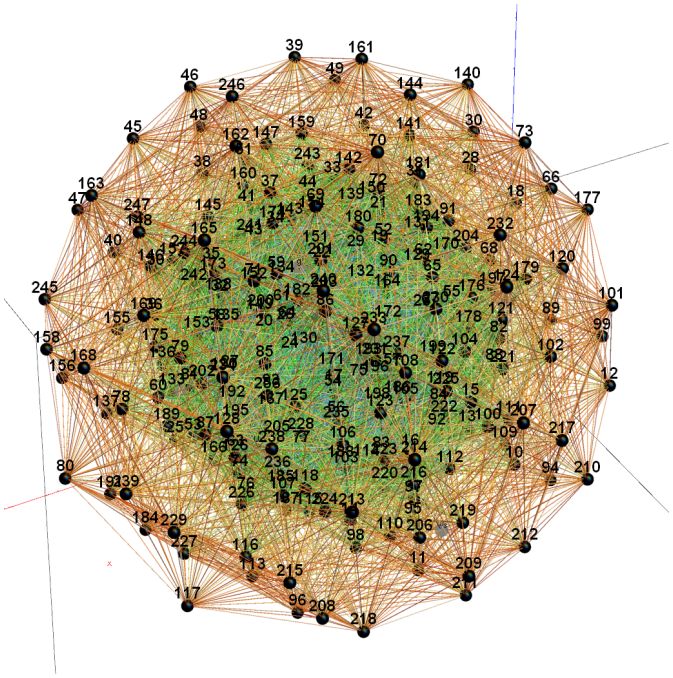

FIG. 5: Vertex numbered E_8 in 3D perspective projection showing 6720 edges of 8D norm of length $\sqrt{2}$

II. THE EDGE GROUP THAT LINKS H_4 TO $H_4\Phi$ ($L \leftrightarrow R$)

It has already been mentioned that a single 8D E_8 vertex (with a pair of L and R 4D entries) always links to another E_8 pair of 4D vertices through the $L \leftrightarrow R$ column's cross-reference index number. By studying the pattern of green and black color-coded E_8 L/R column entries in Appendix A, it becomes clear that the the $L \leftrightarrow R$ index always links between H_4 and $H_4\Phi$ pairs of 4D vertices. Since it has already been shown that the 24-cell $L \leftrightarrow R$ pairs exhibit a symmetry for either self-reference or anti-vertex reference linking H_4 and $H_4\Phi$ 24-cells, this suggests there might be a linking symmetry in the Snub 24-cells as well.

There are 4 Snub 24-cells of 96 vertices each in the rotation of E_8. Interestingly, using the vertex index and the $L \leftrightarrow R$ index to define an edge between the 8D vertices results in a single group of 8D edge norm of length $l = 4\varphi$. Indeed, if we select all 8D edges of norm l from the 28680 edges of the complete graph of the rotated E_8, it results in a group of 168 edge lines. From these, we eliminate the 72 edges where the first edge vertex's L is not equal to the second edge vertex's R (as required for the cross-reference in $L \leftrightarrow R$). The remaining 96 edge vertex pairs are precisely the $2 * 96 = 192$ $L \leftrightarrow R$ vertex pairs of the 4 Snub 24-cells of Appendix A. These are shown in Fig. 6 with each edge line linking the H_4 and $H_4\Phi$ related vertices in the Snub 24-cells.

III. CONSTRUCTING E_8 FROM THE H_4 600-CELL

Dechant suggested[4] that the construction of E_8 from the lower dimensional structures of the Icosahedron, and spinors (Icosians), through the H_4 600-cell is new. Baez has discussed the idea as well[5].

Analyzing [4] using the simple roots matrix $\mathrm{E8_{srm}}$ in (1) as applied to the generation of the Cartan matrix (2), we get similar results. See Fig. 7 for a symbolic analysis using *Mathematica*^{TM}. Note the resulting Cartan matrix after applying $\mathrm{H4_{rot}}$ as a dot product to $\mathrm{E8_{srm}}$ is the same as before rotation after applying Dechant's φ=0 trick, with an interesting exception in the entry at $(5,5) = 4$ and not 2, and (6,5)=(5,6)=-2 and not -1, as they should be.

The detail of the Dechant's construction successfully creates the two scaled L copies of 4D H_4 and $H_4\Phi$ without providing detail on how to associate the other two scaled R copies within the 8D E_8 vertices. This detail is assumed due to the ability to "identify" the folded E_8 Dynkin diagram's structure using 4D H_4 and $H_4\Phi$ elements with each node. It is not clear from that work that there is a prescription for constructing (L,R) 8D E_8 vertices from H_4 and $H_4\Phi$. It seems in both of these works, it is left as a "challenge to the reader" to resolve these details.

In order to resolve that detail, the procedural construction from 4D to 8D would seem to require reference to some form of $\mathrm{H4_{rot}^{-1}}$ dot product applied to the properly associated combination of 240 4D L and R from H_4 and $H_4\Phi$ into

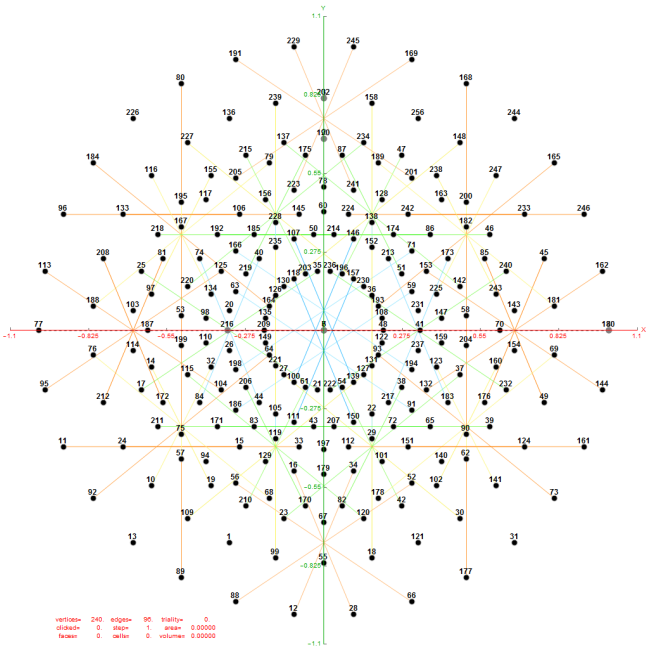

FIG. 6: Vertex numbered Petrie projection of the rotated E_8, showing the 96 edges of 8D norm $l = 4\varphi$ which links the Snub 24-cell H_4 and $H_4\Phi$ ($L \leftrightarrow R$) vertices (Note: the 8 excluded positive E_8 8-Orthoplex (or equivalently, theH_4 and $H_4\Phi$ 4-Orthoplex) "generator vertices" are shown as larger gray labeled axis dots which overlap their darker black E_8 vertices)

.

240 8D (L,R) vertices. From the 240 (L,R) 8D vertices, there are 48 which are easily determined from 24-cell and 24-cellΦ patterns mentioned in Section I-A. For the 24-cell, these are the 24 vertex permutations where the 8-cell $\{\pm\varphi, \pm\varphi, \pm\varphi, \pm\varphi\}$ and 16-cell $\{\pm 2\varphi, 0, 0, 0\}$ all have L=-R. For the 24-cellΦ, these are the 24 vertex permutations where the 8-cellΦ $\{\pm 1, \pm 1, \pm 1, \pm 1\}$ and 16-cellΦ $\{\pm 2, 0, 0, 0\}$ all have L=R.

We also note that it is the $\pm\Phi$ in the vertex that defines its membership in the $H_4\Phi$ 600-cell and remember that it must be exchanged between (L,R) 4D halves with $\pm\varphi^2$.

The introduction of the edge group in Section II that links L and R to H_4 and $H_4\Phi$ ($L \leftrightarrow R$) vertices of the Snub 24-cell is a key detail that can be used to define a procedure to construct the other 192 8D vertices. Specifically, this involves pairing each of the 192 remaining Snub 24-cell permutations of $\{0, \pm 1, \pm\varphi, \pm\varphi^2\}$ from H_4 and Snub 24-cellΦ permutations of $\{0, \pm 1, \mp\varphi, \pm\Phi\}$ from $H_4\Phi$ with some other Snub 24-cell $H_4\Phi$ and H_4 vertex, respectively.

One procedural solution offered is to simply select from the set of $192^2 = 36864$ possible pairwise combinations of (L,R), by choosing only those with a 4φ 8D norm edge length between (L,R) and (R,L) where L$\neq \pm$R as in (6).

$$\text{Norm[(L,R)-(R,L))]} = \sqrt{2}\text{Norm[L-R]} = 4\varphi \tag{6}$$

It is the introduction of $\text{H4}_{\text{rot}}^{-1}$ as a dot product with the identified 8D (L,R) H_4 and $H_4\Phi$ vertices that unlocks the detail of constructing E_8 from the Icosahedron and H_4!

A second even simpler procedure is to notice in Appendix A that the permutations of each dimension of the L and R always maintain the dimensional positions for 0, $\pm$ 1, and $\pm\varphi \leftrightarrow \mp\varphi$ between them. Combining this insight with knowing that (L,R) must now exchange $\pm\varphi^2 \leftrightarrow \pm\Phi$, we have a simple prescription for constructing (L,R) for the Snub 24-cell vertices based on knowing only L or R. Yet, it is not obvious that this prescription is predicted by Dechant's work.

IV. CONCENTRIC PLATONIC SOLID HULLS OF E_8 AND H_4

By selecting a 3D projection basis for E_8 from rows 2 through 4 of H4_{rot} and sorting the resulting projected vertex positions into groups based on its 3D norm position, a pattern of 14 Platonic solid hulls in 7 Φ scaled pairs emerges with 4 points at the origin, as shown in Fig. 8. Listing these from smallest norm to largest, we have for the smaller

▼ a) Resulting Cartan matrix before applying $H4_{rot}$ rotation

In[3]:= $E8_{srm} \cdot E8_{srm}^{T}$

Out[3]=
$$\begin{pmatrix} 2 & -1 & 0 & 0 & 0 & 0 & 0 & 0 \\ -1 & 2 & -1 & 0 & 0 & 0 & 0 & 0 \\ 0 & -1 & 2 & -1 & 0 & 0 & 0 & 0 \\ 0 & 0 & -1 & 2 & 0 & 0 & -1 & 0 \\ 0 & 0 & 0 & 0 & 2 & -1 & 0 & 0 \\ 0 & 0 & 0 & 0 & -1 & 2 & -1 & 0 \\ 0 & 0 & 0 & -1 & 0 & -1 & 2 & -1 \\ 0 & 0 & 0 & 0 & 0 & 0 & -1 & 2 \end{pmatrix}$$

▼ b) Generating the rotated Cartan matrix from SRM and $H4_{rot}$ in symbolic form

In[4]:= $\text{FullSimplify}[(E8_{srm} \cdot H4_{rot}) \cdot (E8_{srm} \cdot H4_{rot})^{T} / 2]$

Out[4]=
$$\begin{pmatrix} \frac{1}{2}(\varphi^4 + 2\varphi^2 + \Phi^2 + 2) & -\varphi^2 - 1 & 0 & -\varphi^2 \Phi & -\frac{1}{4}(\varphi^2 + \Phi - 2)(\varphi^2 + \Phi + 2) & \varphi^2 - 1 & (\Phi - 1)\varphi^2 + 1 & \varphi^2 - 1 \\ -\varphi^2 - 1 & 2(\varphi^2 + 1) & -\varphi^2 - 1 & 0 & 0 & 0 & \varphi^2 - 1 & 2 - 2\varphi^2 \\ 0 & -\varphi^2 - 1 & 2(\varphi^2 + 1) & -\varphi^2 - 1 & 0 & 1 - \varphi^2 & 0 & \varphi^2 - 1 \\ -\varphi^2 \Phi & 0 & -\varphi^2 - 1 & \frac{1}{2}(\varphi^4 + 2\varphi^2 + \Phi^2 + 2) & \frac{1}{4}(\varphi^2 + \Phi - 2)(\varphi^2 + \Phi + 2) & 0 & \frac{1}{2}(-\varphi^4 - \Phi^2) & 0 \\ -\frac{1}{4}(\varphi^2 + \Phi - 2)(\varphi^2 + \Phi + 2) & 0 & 0 & \frac{1}{4}(\varphi^2 + \Phi - 2)(\varphi^2 + \Phi + 2) & \frac{1}{4}((\varphi^2 + \Phi)^2 + 12) & -2 & -\frac{1}{4}(\varphi^2 + \Phi - 2)(\varphi^2 + \Phi + 2) & 0 \\ \varphi^2 - 1 & 0 & 1 - \varphi^2 & 0 & -2 & 2(\varphi^2 + 1) & -\varphi^2 - 1 & 0 \\ (\Phi - 1)\varphi^2 + 1 & \varphi^2 - 1 & 0 & \frac{1}{2}(-\varphi^4 - \Phi^2) & -\frac{1}{4}(\varphi^2 + \Phi - 2)(\varphi^2 + \Phi + 2) & -\varphi^2 - 1 & \frac{1}{2}(\varphi^4 + 2\varphi^2 + \Phi^2 + 2) & -\varphi^2 - 1 \\ \varphi^2 - 1 & 2 - 2\varphi^2 & \varphi^2 - 1 & 0 & 0 & 0 & -\varphi^2 - 1 & 2(\varphi^2 + 1) \end{pmatrix}$$

▼ c) Replacing symbols with the mathematical representation is required due to unique degeneracy within the Golden Ratio

In[5]:= $\text{FullSimplify}\left[\% /. \left\{\Phi \to \frac{1}{2}\left(1 + \sqrt{5}\right), \varphi \to \frac{1}{2}\left(\sqrt{5} - 1\right)\right\}\right]$

Out[5]=
$$\begin{pmatrix} 5 - \sqrt{5} & \frac{1}{2}(-5 + \sqrt{5}) & 0 & \frac{1}{2}(1 - \sqrt{5}) & 0 & \frac{1}{2}(1 - \sqrt{5}) & -1 + \sqrt{5} & \frac{1}{2}(1 - \sqrt{5}) \\ \frac{1}{2}(-5 + \sqrt{5}) & 5 - \sqrt{5} & \frac{1}{2}(-5 + \sqrt{5}) & 0 & 0 & 0 & \frac{1}{2}(1 - \sqrt{5}) & -1 + \sqrt{5} \\ 0 & \frac{1}{2}(-5 + \sqrt{5}) & 5 - \sqrt{5} & \frac{1}{2}(-5 + \sqrt{5}) & 0 & \frac{1}{2}(-1 + \sqrt{5}) & 0 & \frac{1}{2}(1 - \sqrt{5}) \\ \frac{1}{2}(1 - \sqrt{5}) & 0 & \frac{1}{2}(-5 + \sqrt{5}) & 5 - \sqrt{5} & 0 & 0 & \frac{1}{2}(-5 + \sqrt{5}) & 0 \\ 0 & 0 & 0 & 0 & 4 & -2 & 0 & 0 \\ \frac{1}{2}(1 - \sqrt{5}) & 0 & \frac{1}{2}(-1 + \sqrt{5}) & 0 & -2 & 5 - \sqrt{5} & \frac{1}{2}(-5 + \sqrt{5}) & 0 \\ -1 + \sqrt{5} & \frac{1}{2}(1 - \sqrt{5}) & 0 & \frac{1}{2}(-5 + \sqrt{5}) & 0 & \frac{1}{2}(-5 + \sqrt{5}) & 5 - \sqrt{5} & \frac{1}{2}(-5 + \sqrt{5}) \\ \frac{1}{2}(1 - \sqrt{5}) & -1 + \sqrt{5} & \frac{1}{2}(1 - \sqrt{5}) & 0 & 0 & 0 & \frac{1}{2}(-5 + \sqrt{5}) & 5 - \sqrt{5} \end{pmatrix}$$

▼ d) Replacing reduced mathematical values back to symbols showing some of the E_8 Cartan matrix patterns

In[6]:=
```
% /. {
  -1 + √5 → 2 φ,
  1 - √5 → -2 φ,
  5 - √5 → 2 (φ^2 + 1),
  -5 + √5 → -2 (φ^2 + 1)}
```

Out[6]=
$$\begin{pmatrix} 2(\varphi^2 + 1) & -\varphi^2 - 1 & 0 & -\varphi & 0 & -\varphi & 2\varphi & -\varphi \\ -\varphi^2 - 1 & 2(\varphi^2 + 1) & -\varphi^2 - 1 & 0 & 0 & 0 & -\varphi & 2\varphi \\ 0 & -\varphi^2 - 1 & 2(\varphi^2 + 1) & -\varphi^2 - 1 & 0 & \varphi & 0 & -\varphi \\ -\varphi & 0 & -\varphi^2 - 1 & 2(\varphi^2 + 1) & 0 & 0 & -\varphi^2 - 1 & 0 \\ 0 & 0 & 0 & 0 & 4 & -2 & 0 & 0 \\ -\varphi & 0 & \varphi & 0 & -2 & 2(\varphi^2 + 1) & -\varphi^2 - 1 & 0 \\ 2\varphi & -\varphi & 0 & -\varphi^2 - 1 & 0 & -\varphi^2 - 1 & 2(\varphi^2 + 1) & -\varphi^2 - 1 \\ -\varphi & 2\varphi & -\varphi & 0 & 0 & 0 & -\varphi^2 - 1 & 2(\varphi^2 + 1) \end{pmatrix}$$

▼ e) Performing Dechant's $\varphi \to 0$ trick regains our E_8 Cartan matrix pattern, albeit with an (5,5)=4 (not 2), and (6,5)=(5,6)=-2 (not -1)

In[7]:= $\% /. \{\varphi \to 0\}$

Out[7]=
$$\begin{pmatrix} 2 & -1 & 0 & 0 & 0 & 0 & 0 & 0 \\ -1 & 2 & -1 & 0 & 0 & 0 & 0 & 0 \\ 0 & -1 & 2 & -1 & 0 & 0 & 0 & 0 \\ 0 & 0 & -1 & 2 & 0 & 0 & -1 & 0 \\ 0 & 0 & 0 & 0 & 4 & -2 & 0 & 0 \\ 0 & 0 & 0 & 0 & -2 & 2 & -1 & 0 \\ 0 & 0 & 0 & -1 & 0 & -1 & 2 & -1 \\ 0 & 0 & 0 & 0 & 0 & 0 & -1 & 2 \end{pmatrix}$$

FIG. 7: Symbolic analysis using *Mathematica*^{TM} comparing the Cartan matrix before and after rotating the simple roots matrix $E8_{srm}$ used to create it (Note: the resulting Cartan matrix is not precisely that of E_8, even after applying the Dechant $\varphi = 0$ trick)

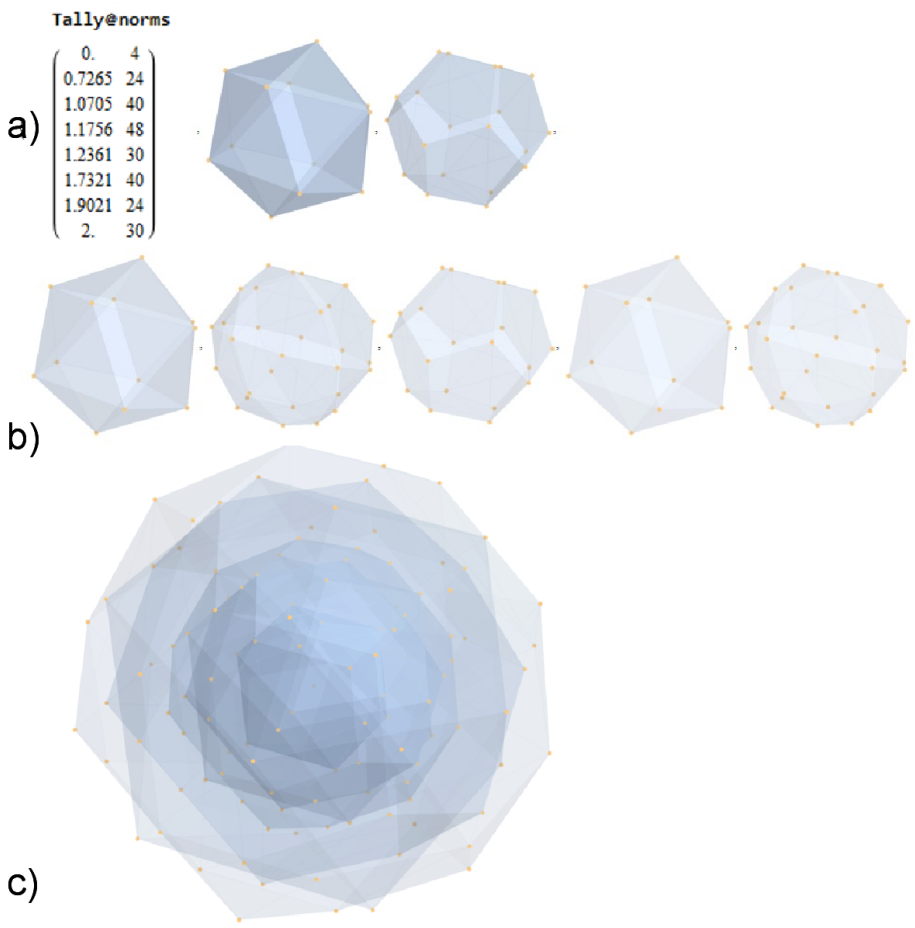

FIG. 8: a) Sorted list of the vertex norms with their grouped vertex counts. b) 3D surface models for each of the 7 hulls of vertices c) Combined 3D surface model with increasing transparency for each successive hull.

H_4; 2 Icosahedrons, 2 Dodecahedrons, and 2 Icosahedrons from a group of 4. We finish the smaller H_4 with an IcosaDodecahedron. The larger scaled $H_4\Phi$ has 2 Icosahedrons from the previously mentioned group of 4 and adds 2 Dodecahedrons, 2 Icosahedrons, and the outer IcosaDodecahedron hull.

It is an interesting exercise to apply this concentric hull creation procedure on the sub-group structures of E_8 (such as D_8, BC_8, E_7, E_6, D_6, BC_6). For example, the 112 integer vertex D_8 projects to one pair of Φ scaled (outer and interior) hulls of the 30 vertex IcosaDodecahedrons and two pairs of Φ scaled (outer and interior) hulls 12 vertex Icosahedrons, with 4 vertices at the origin. Similarly, the $2^7 = 128$ $\frac{1}{2}$ integer vertices of BC_8 (a.k.a. the 8-DemiCube or 7-cube) projects to two pairs of Φ scaled (outer and interior) hulls of 32 vertex Rhombic Triacontahedrons (each made of an Icosahedron and a Dodecahedron). The 8 grouped sets of hull vertices in E_8 split across the integer (Bosons) and $\frac{1}{2}$ integer Fermions as assigned in [3]. These are shown in Figs. 9-10, respectively.

The two scaled 30 vertex IcosaDodecahedrons mentioned are isomorphic to the 60 vertex D_6.

V. PLATONIC SOLID CRYSTAL PROJECTION PRISMS

In analyzing the 3 basis vectors from Section IV (rows 2 through 4 of $\mathrm{H4_{rot}}$ used in projecting the Platonic solid hulls), we find that by taking the transpose of the 3×8 basis vector matrix, the results are 8 3D vertex locations with 2 at the origin. Adding their anti-vertices (i.e. their negation, as in rows 6 through 8 of $\mathrm{H4_{rot}}$) results in a very symmetric construction of the Icosahedron from 3 Golden Rectangles aligned along orthonormal axial planes as shown in Fig. 1 of [5] (originally obtained from Wikipedia commons). So in a sense, the Platonic solid's Icosahedron becomes a "crystal projection prism" through which we get a 3D projection of the entire structure of E_8. This projection results in seven Φ scaled pairs of Icosahedrons, Dodecahedrons, and IcosaDodecahedrons, with an 8th "scaled pair of 2 vertices" at the origin coming from the pair of vertices at the origin in our basis vectors. Any 3D

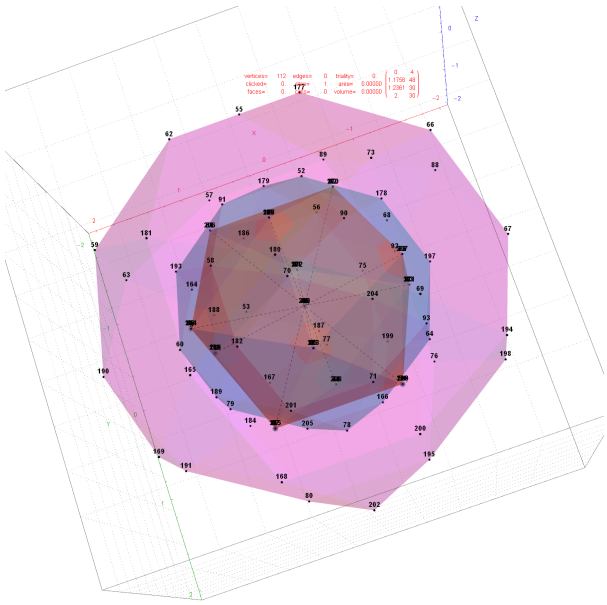

FIG. 9: Numbered 112 integer vertex D_8 perspective projected into a combined 3D surface model of hulls with increasing transparency for each successive hull, including the list of the vertex norms with their grouped vertex counts

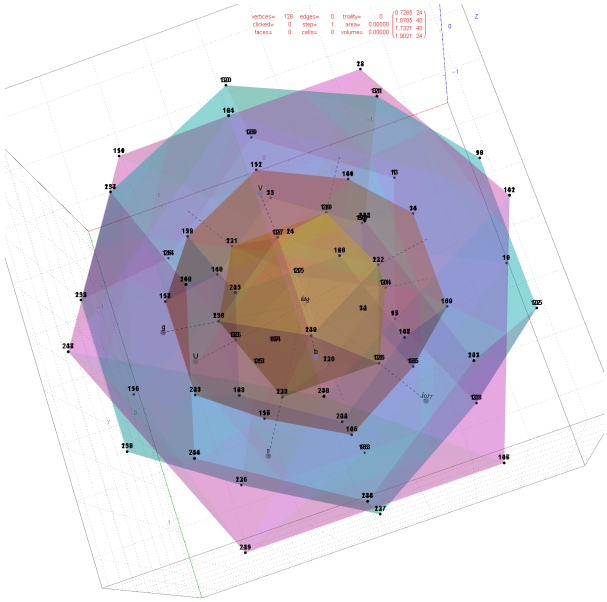

FIG. 10: Numbered 128 $\frac{1}{2}$ integer vertex BC_8 perspective projected into a combined 3D surface model of hulls with increasing transparency for each successive hull, including the list of the vertex norms with their grouped vertex counts

rotation of any set of 6 Icosahedron vertices (or 6 anti-vertices) combined with 2 at the origin (in any order) can be used as a crystal projection prism to produce this sequence of 8 pairs of Platonic solid hulls.

An alternative perspective is to look at E_8 after being rotated into H_4 and $H_4\Phi$ vertices. Any set of 3D orthonormal projection basis from the L or R 4D halves provide for the same results, as shown in Fig. 11. Notice the vertex norm group counts are identical to those in Fig. 8, but the image is rotated and scaled differently as expected.

It should also be noted that the Icosahedron as basis vectors used in projecting E_8 to 3D is explicitly represented in the projections as the 16 8-Orthoplex excluded "generator vertices" with 4 at the origin. These can be seen as 8 positive labeled dotted line axis vectors in the diagrams with the "anti-generator' vertices" being the tail of the positive axis vector. In this particular projection basis, these axis vertices overlap the included 8-Orthoplex vertices which are part of the 240 vertices in E_8, indicating a special relationship between the generators and vertices wthin

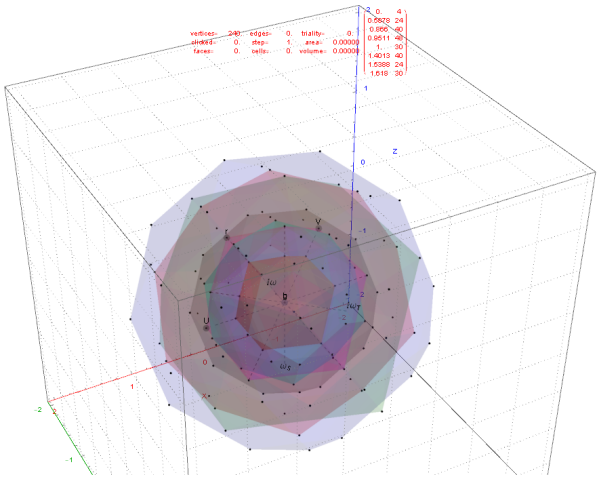

FIG. 11: 3D projection using an orthonormal basis on H_4 and $H_4\Phi$ vertices (i.e. the rotated E_8)

this particular projection basis. Please note that the rotated vertices do not all maintain the same non-zero index location when they rotate from E_8 to H_4 and $H_4\Phi$. See the red and orange highlighted rows in Appendix A for more detail.

This process of taking 8 selected points from symmetric 3D objects and creating E_8 projection prism basis vectors out of their transposed matrix produces a few interesting (read symmetric) concentric hull sets of objects. A few examples are shown in Appendix B Figs. 13-15, each with: a) the crystal prism geometry and vertices, b) the selected basis vectors, c) the individual 3D projected concentric hull objects, d) the combined set of concentric objects with progressively increasing transparency and tally of vertex norms. These figures also highlight the vertices with size, shape, and color based on algorithms that take advantage of the L/R structure of E_8. More detail on the algorithm for this assignment is provided in [3].

There are non-Platonic solid prisms that also create interesting concentric hull patterns from E_8. Some of these are the MetabidiminishedIcosahedron (with its negated vertices gives the GyroelongatedPentagonalPyramid), the Cuboctahedron, and the RhombicDodecahedron. These are shown in Appendix B Figs. 16-18.

VI. THE TETRAHELIX EMERGING FROM 8 CONCENTRIC RINGS OF 30 E_8 AND H_4+$H_4\Phi$ VERTICES

The Boerdijk-Coxeter helix (a.k.a. Tetrahelix) is also related to these structures through the Golden Ratio. It is a 4D helix (of 3D tetrahedral cells) that makes up the vertices on the 8 concentric rings of E_8 Petrie projection (or the H4 and H4 rings of the two 600 cells in E_8).

From Wikipedia "The 600-cell partitions into 20 rings of 30 tetrahedra, each a BoerdijkCoxeter helix. When superimposed onto the 3-sphere curvature it becomes periodic, with a period of ten vertices, encompassing all 30 cells. The collective of such helices in the 600-cell represent a discrete Hopf fibration. While in 3 dimensions the edges are helices, in the imposed 3-sphere topology they are geodesics and have no torsion. They spiral around each other naturally due to the Hopf fibration. In addition, the 16-cell partitions into two 8-tetrahedron rings, four edges long, and the 5-cell partitions into a single degenerate 5-tetrahedron ring."

The tetrahedral cell faces and 3D vertex shape-color-size based on quantum particle parameters from a theoretical physics model are shown in Fig. 12. The Beordijk-Coxeter helix connects the nearest 6 vertices on the outer ring.

VII. CONCLUSION

Instead of simply folding the 8D E_8 vertices into 4D pairs of H_4 and $H_4\Phi$ vertices, we rotated them using an 8×8 matrix. This transforms E_8 into a fourfold H_4 600-cell structure. This was deconstructed into the 40 individual 16 vertex Tesseracts and 8 vertex 4-Orthoplexes. By projecting these structures into 2D and 3D visualizations, a better understanding of the symmetry relationships within E_8 was studied. In addition to showing that the base 24-cell structures have an independent (self referencing) existence within H_4 and $H_4\Phi$, an edge group of norm 2φ was found to describe the detail of the Snub 24-cells' link between H_4 and $H_4\Phi$ ($L \leftrightarrow R$). Using that discovery, a more

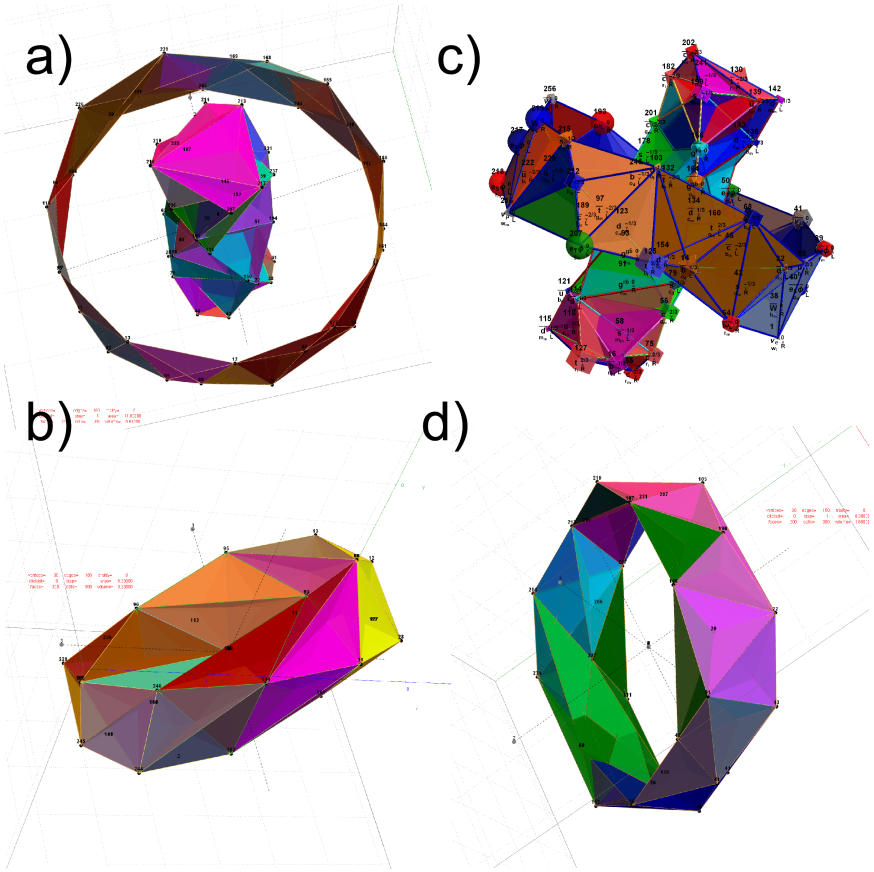

FIG. 12: The Beordijk-Coxeter Tetrahelix emerging from the 8 concentric rings of 30 E_8 and H_4+$H_4\Phi$ Petrie projection vertices; a) $H_4\Phi$ inner and outer ring in 3D, b) with vertex size, shape, color assigned from physics model, c-d) inner and outer ring in orthonormal projection of $H_4\Phi$

explicit procedure and basis for constructing E_8 from H_4 has been given. Highlighting the relationship between the vertices of an Icosahedron, the rotation matrix, and the 3D projection basis for the concentric hulls of E_8, eight pairs of concentric hulls of Platonic solids were identified. We show that the symmetries of various geometric structures, including all of the Platonic solids, function as 3D crystal projection prisms. Finally, we visualized Beordijk-Coxeter Tetrahelix emerging from the Petrie projection's concentric rings of 30 vertices of the H_4 600-cells.

Acknowledgments

I would like to thank my wife for her love and patience and those in academia who have taken the time to review this work.

[1] M. Koca and N. Koca, Turkish Journal of Physics **22**, 421 (1998).
[2] D. A. Richter, ArXiv e-prints math.GM/0704.3091 (2007), 0704.3091.
[3] J. G. Moxness, `www.vixra.org/abs/1411.0130` (2014).
[4] P.-P. Dechant, Proceedings of the Royal Society of London Series A **472**, 20150504 (2016), 1602.05985.
[5] J. C. Baez, ArXiv e-prints (2017), 1712.06436.

APPENDIX A: LIST OF E_8 AND ITS ROTATED H_4 AND $H_4\Phi$ VERTICES

This table splits the E_8 and its rotated H_4 vertices into L/R 4D elements.

1. Table structure

The first column is an SRE E_8 vertex index number derived from sorting the E_8 vertices by their position based on the $256 = 2^8$ binary pattern from the 9th row of the Pascal triangle {1, 8, 28, 56, 70, 56, 28, 8, 1} and its associated Cl_8 Clifford Algebra. This construction is described in more detail in [3]. The odd groups (1,3,5,7,9) with (1,26,70,26,1) elements (respectively) are the 128 $\frac{1}{2}$ integer vertices. The even groups (2,4,6,8) with (8,56,56,8) elements (respectively) are the 112 integer vertices along with the 16 excluded 8 generator (and 8 anti-generator) vertices (2-9 and 248-255) with permutations of $\{\pm 1, 0, 0, 0, 0, 0, 0, 0\}$ (a.k.a. the 8-Orthoplex), such that they indicate the basis vectors used for projecting the polytope.

Only the first half of the 240 vertices is shown, since the last half is simply the reverse order negation of the vertices in the first half (e.g. the E_8 vertex $n = 10$ has as its' negation $257 - n = 247$).

The middle column labeled L↔R indicates the vertex reference number that contains the same L as the R (and equivalently, the same R as the L, interestingly enough).

2. Table color coding

The E_8 L/R columns' green color-coded elements indicate that the 4D vertex rotates into the smaller H_4 600-cell. Conversely, the E_8 L/R columns' black color-coded elements indicate the 4D vertex rotates into the larger $H_4\Phi$ 600-cell.

The H_4 L/R columns' red color-coded rows are 24-cell elements that always self-reference and are always members of the scaled up 600-cell $H_4\Phi$. The H_4 L/R columns' orange color-coded rows are 24-cell elements that always reference the negated elements in the range of 129-256 and are always members of the smaller 600-cell H_4.

#	E8 L	H4 L	L↔R	H4 R	E8 R
1	$\left\{-\frac{1}{2},-\frac{1}{2},-\frac{1}{2},-\frac{1}{2}\right\}$	{1, 1, 1, 1}	1	{1, 1, 1, 1}	$\left\{-\frac{1}{2},-\frac{1}{2},-\frac{1}{2},-\frac{1}{2}\right\}$
10	$\left\{\frac{1}{2},\frac{1}{2},-\frac{1}{2},-\frac{1}{2}\right\}$	{−φ, Φ, 0, 1}	32	{φ, φ², 0, 1}	$\left\{-\frac{1}{2},-\frac{1}{2},-\frac{1}{2},-\frac{1}{2}\right\}$
11	$\left\{\frac{1}{2},-\frac{1}{2},\frac{1}{2},-\frac{1}{2}\right\}$	{−φ, 0, 1, Φ}	33	{φ, 0, 1, φ²}	$\left\{-\frac{1}{2},-\frac{1}{2},-\frac{1}{2},-\frac{1}{2}\right\}$
12	$\left\{\frac{1}{2},-\frac{1}{2},-\frac{1}{2},\frac{1}{2}\right\}$	{−φ, 1, Φ, 0}	34	{φ, 1, φ², 0}	$\left\{-\frac{1}{2},-\frac{1}{2},-\frac{1}{2},-\frac{1}{2}\right\}$
13	$\left\{\frac{1}{2},-\frac{1}{2},-\frac{1}{2},-\frac{1}{2}\right\}$	{−1, 1, 1, 1}	13	{−1, 1, 1, 1}	$\left\{\frac{1}{2},-\frac{1}{2},-\frac{1}{2},-\frac{1}{2}\right\}$
14	$\left\{\frac{1}{2},-\frac{1}{2},-\frac{1}{2},-\frac{1}{2}\right\}$	{−φ, φ², 0, 1}	19	{φ, Φ, 0, 1}	$\left\{-\frac{1}{2},\frac{1}{2},-\frac{1}{2},-\frac{1}{2}\right\}$
15	$\left\{\frac{1}{2},-\frac{1}{2},-\frac{1}{2},-\frac{1}{2}\right\}$	{−φ, 0, 1, φ²}	24	{φ, 0, 1, Φ}	$\left\{-\frac{1}{2},-\frac{1}{2},\frac{1}{2},-\frac{1}{2}\right\}$
16	$\left\{\frac{1}{2},-\frac{1}{2},-\frac{1}{2},-\frac{1}{2}\right\}$	{−φ, 1, φ², 0}	28	{φ, 1, Φ, 0}	$\left\{-\frac{1}{2},-\frac{1}{2},-\frac{1}{2},\frac{1}{2}\right\}$
17	$\left\{-\frac{1}{2},\frac{1}{2},\frac{1}{2},-\frac{1}{2}\right\}$	{1, φ, 0, Φ}	35	{1, −φ, 0, φ²}	$\left\{-\frac{1}{2},-\frac{1}{2},-\frac{1}{2},-\frac{1}{2}\right\}$
18	$\left\{-\frac{1}{2},\frac{1}{2},-\frac{1}{2},\frac{1}{2}\right\}$	{1, Φ, φ, 0}	36	{1, φ², −φ, 0}	$\left\{-\frac{1}{2},-\frac{1}{2},-\frac{1}{2},-\frac{1}{2}\right\}$
19	$\left\{-\frac{1}{2},\frac{1}{2},-\frac{1}{2},-\frac{1}{2}\right\}$	{φ, Φ, 0, 1}	14	{−φ, φ², 0, 1}	$\left\{\frac{1}{2},-\frac{1}{2},-\frac{1}{2},-\frac{1}{2}\right\}$
20	$\left\{-\frac{1}{2},\frac{1}{2},-\frac{1}{2},-\frac{1}{2}\right\}$	{1, 1, −1, 1}	20	{1, 1, −1, 1}	$\left\{-\frac{1}{2},\frac{1}{2},-\frac{1}{2},-\frac{1}{2}\right\}$
21	$\left\{-\frac{1}{2},\frac{1}{2},-\frac{1}{2},-\frac{1}{2}\right\}$	{1, φ, 0, φ²}	25	{1, −φ, 0, Φ}	$\left\{-\frac{1}{2},-\frac{1}{2},\frac{1}{2},-\frac{1}{2}\right\}$
22	$\left\{-\frac{1}{2},\frac{1}{2},-\frac{1}{2},-\frac{1}{2}\right\}$	{1, Φ, −φ, 0}	29	{1, φ², φ, 0}	$\left\{-\frac{1}{2},-\frac{1}{2},-\frac{1}{2},\frac{1}{2}\right\}$
23	$\left\{-\frac{1}{2},-\frac{1}{2},\frac{1}{2},\frac{1}{2}\right\}$	{1, 0, Φ, φ}	37	{1, 0, φ², −φ}	$\left\{-\frac{1}{2},-\frac{1}{2},-\frac{1}{2},-\frac{1}{2}\right\}$
24	$\left\{-\frac{1}{2},-\frac{1}{2},\frac{1}{2},-\frac{1}{2}\right\}$	{φ, 0, 1, Φ}	15	{−φ, 0, 1, φ²}	$\left\{\frac{1}{2},-\frac{1}{2},-\frac{1}{2},-\frac{1}{2}\right\}$
25	$\left\{-\frac{1}{2},-\frac{1}{2},\frac{1}{2},-\frac{1}{2}\right\}$	{1, −φ, 0, Φ}	21	{1, φ, 0, φ²}	$\left\{-\frac{1}{2},\frac{1}{2},-\frac{1}{2},-\frac{1}{2}\right\}$
26	$\left\{-\frac{1}{2},-\frac{1}{2},\frac{1}{2},-\frac{1}{2}\right\}$	{1, −1, 1, 1}	26	{1, −1, 1, 1}	$\left\{-\frac{1}{2},-\frac{1}{2},\frac{1}{2},-\frac{1}{2}\right\}$
27	$\left\{-\frac{1}{2},-\frac{1}{2},\frac{1}{2},-\frac{1}{2}\right\}$	{1, 0, φ², φ}	30	{1, 0, Φ, −φ}	$\left\{-\frac{1}{2},-\frac{1}{2},-\frac{1}{2},\frac{1}{2}\right\}$
28	$\left\{-\frac{1}{2},-\frac{1}{2},-\frac{1}{2},\frac{1}{2}\right\}$	{φ, 1, Φ, 0}	16	{−φ, 1, φ², 0}	$\left\{\frac{1}{2},-\frac{1}{2},-\frac{1}{2},-\frac{1}{2}\right\}$
29	$\left\{-\frac{1}{2},-\frac{1}{2},-\frac{1}{2},\frac{1}{2}\right\}$	{1, φ², φ, 0}	22	{1, Φ, −φ, 0}	$\left\{-\frac{1}{2},\frac{1}{2},-\frac{1}{2},-\frac{1}{2}\right\}$
30	$\left\{-\frac{1}{2},-\frac{1}{2},-\frac{1}{2},\frac{1}{2}\right\}$	{1, 0, Φ, −φ}	27	{1, 0, φ², φ}	$\left\{-\frac{1}{2},-\frac{1}{2},\frac{1}{2},-\frac{1}{2}\right\}$
31	$\left\{-\frac{1}{2},-\frac{1}{2},-\frac{1}{2},\frac{1}{2}\right\}$	{1, 1, 1, −1}	31	{1, 1, 1, −1}	$\left\{-\frac{1}{2},-\frac{1}{2},-\frac{1}{2},\frac{1}{2}\right\}$
32	$\left\{-\frac{1}{2},-\frac{1}{2},-\frac{1}{2},-\frac{1}{2}\right\}$	{φ, φ², 0, 1}	10	{−φ, Φ, 0, 1}	$\left\{\frac{1}{2},\frac{1}{2},-\frac{1}{2},-\frac{1}{2}\right\}$
33	$\left\{-\frac{1}{2},-\frac{1}{2},-\frac{1}{2},-\frac{1}{2}\right\}$	{φ, 0, 1, φ²}	11	{−φ, 0, 1, Φ}	$\left\{\frac{1}{2},-\frac{1}{2},\frac{1}{2},-\frac{1}{2}\right\}$
34	$\left\{-\frac{1}{2},-\frac{1}{2},-\frac{1}{2},-\frac{1}{2}\right\}$	{φ, 1, φ², 0}	12	{−φ, 1, Φ, 0}	$\left\{\frac{1}{2},-\frac{1}{2},-\frac{1}{2},\frac{1}{2}\right\}$
35	$\left\{-\frac{1}{2},-\frac{1}{2},-\frac{1}{2},-\frac{1}{2}\right\}$	{1, −φ, 0, φ²}	17	{1, φ, 0, Φ}	$\left\{-\frac{1}{2},\frac{1}{2},\frac{1}{2},-\frac{1}{2}\right\}$
36	$\left\{-\frac{1}{2},-\frac{1}{2},-\frac{1}{2},-\frac{1}{2}\right\}$	{1, φ², −φ, 0}	18	{1, Φ, φ, 0}	$\left\{-\frac{1}{2},\frac{1}{2},-\frac{1}{2},\frac{1}{2}\right\}$
37	$\left\{-\frac{1}{2},-\frac{1}{2},-\frac{1}{2},-\frac{1}{2}\right\}$	{1, 0, φ², −φ}	23	{1, 0, Φ, φ}	$\left\{-\frac{1}{2},-\frac{1}{2},\frac{1}{2},\frac{1}{2}\right\}$
38	{−1, −1, 0, 0}	{Φ, −φ, 1, 0}	82	{φ², φ, 1, 0}	{0, 0, 0, 0}
39	{−1, 0, −1, 0}	{Φ, 1, 0, −φ}	83	{φ², 1, 0, φ}	{0, 0, 0, 0}
40	{−1, 0, 0, −1}	{Φ, 0, −φ, 1}	84	{φ², 0, φ, 1}	{0, 0, 0, 0}
41	{−1, 0, 0, 0}	{2, 0, 0, 0}	41	{2, 0, 0, 0}	{−1, 0, 0, 0}
42	{−1, 0, 0, 0}	{Φ, φ, 1, 0}	54	{φ², −φ, 1, 0}	{0, −1, 0, 0}
43	{−1, 0, 0, 0}	{Φ, 1, 0, φ}	65	{φ², 1, 0, −φ}	{0, 0, −1, 0}
44	{−1, 0, 0, 0}	{Φ, 0, φ, 1}	74	{φ², 0, −φ, 1}	{0, 0, 0, −1}
45	{−1, 0, 0, 0}	{Φ, 0, −φ, −1}	176	{φ², 0, φ, −1}	{0, 0, 0, 1}
46	{−1, 0, 0, 0}	{Φ, −1, 0, −φ}	185	{φ², −1, 0, φ}	{0, 0, 1, 0}
47	{−1, 0, 0, 0}	{Φ, −φ, −1, 0}	196	{φ², φ, −1, 0}	{0, 1, 0, 0}
48	{−1, 0, 0, 0}	{2 φ, 0, 0, 0}	209	{−2 φ, 0, 0, 0}	{1, 0, 0, 0}
49	{−1, 0, 0, 1}	{Φ, 0, φ, −1}	85	{φ², 0, −φ, −1}	{0, 0, 0, 0}
50	{−1, 0, 1, 0}	{Φ, −1, 0, φ}	86	{φ², −1, 0, −φ}	{0, 0, 0, 0}
51	{−1, 1, 0, 0}	{Φ, φ, −1, 0}	87	{φ², −φ, −1, 0}	{0, 0, 0, 0}
52	{0, −1, −1, 0}	{0, φ², 1, −φ}	88	{0, Φ, 1, φ}	{0, 0, 0, 0}
53	{0, −1, 0, −1}	{0, −φ, φ², 1}	89	{0, φ, Φ, 1}	{0, 0, 0, 0}
54	{0, −1, 0, 0}	{φ², −φ, 1, 0}	42	{Φ, φ, 1, 0}	{−1, 0, 0, 0}
55	{0, −1, 0, 0}	{0, 0, 2, 0}	55	{0, 0, 2, 0}	{0, −1, 0, 0}
56	{0, −1, 0, 0}	{0, φ², 1, φ}	66	{0, Φ, 1, −φ}	{0, 0, −1, 0}
57	{0, −1, 0, 0}	{0, −φ, Φ, 1}	75	{0, φ, φ², 1}	{0, 0, 0, −1}
58	{0, −1, 0, 0}	{0, −φ, φ², −1}	177	{0, φ, Φ, −1}	{0, 0, 0, 1}
59	{0, −1, 0, 0}	{0, −Φ, 1, −φ}	186	{0, −φ², 1, φ}	{0, 0, 1, 0}
60	{0, −1, 0, 0}	{0, −2 φ, 0, 0}	197	{0, 2 φ, 0, 0}	{0, 1, 0, 0}
61	{0, −1, 0, 0}	{−φ², −φ, 1, 0}	210	{−Φ, φ, 1, 0}	{1, 0, 0, 0}
62	{0, −1, 0, 1}	{0, −φ, Φ, −1}	90	{0, φ, φ², −1}	{0, 0, 0, 0}
63	{0, −1, 1, 0}	{0, −Φ, 1, φ}	91	{0, −φ², 1, −φ}	{0, 0, 0, 0}
64	{0, 0, −1, −1}	{0, 1, −φ, φ²}	92	{0, 1, φ, Φ}	{0, 0, 0, 0}
65	{0, 0, −1, 0}	{φ², 1, 0, −φ}	43	{Φ, 1, 0, φ}	{−1, 0, 0, 0}
66	{0, 0, −1, 0}	{0, Φ, 1, −φ}	56	{0, φ², 1, φ}	{0, −1, 0, 0}
67	{0, 0, −1, 0}	{0, 2, 0, 0}	67	{0, 2, 0, 0}	{0, 0, −1, 0}
68	{0, 0, −1, 0}	{0, 1, φ, φ²}	76	{0, 1, −φ, Φ}	{0, 0, 0, −1}
69	{0, 0, −1, 0}	{0, 1, −φ, −Φ}	178	{0, 1, φ, −φ²}	{0, 0, 0, 1}

#	E8 L	H4 L	L↔R	H4 R	E8 R
70	{0, 0, −1, 0}	{0, 0, 0, −2 φ}	187	{0, 0, 0, 2 φ}	{0, 0, 1, 0}
71	{0, 0, −1, 0}	{0, φ², −1, −φ}	198	{0, Φ, −1, φ}	{0, 1, 0, 0}
72	{0, 0, −1, 0}	{−φ², 1, 0, −φ}	211	{−Φ, 1, 0, φ}	{1, 0, 0, 0}
73	{0, 0, −1, 1}	{0, 1, φ, −Φ}	93	{0, 1, −φ, −φ²}	{0, 0, 0, 0}
74	{0, 0, 0, −1}	{φ², 0, −φ, 1}	44	{Φ, 0, φ, 1}	{−1, 0, 0, 0}
75	{0, 0, 0, −1}	{0, φ, φ², 1}	57	{0, −φ, Φ, 1}	{0, −1, 0, 0}
76	{0, 0, 0, −1}	{0, 1, −φ, Φ}	68	{0, 1, φ, φ²}	{0, 0, −1, 0}
77	{0, 0, 0, −1}	{0, 0, 0, 2}	77	{0, 0, 0, 2}	{0, 0, 0, −1}
78	{0, 0, 0, −1}	{0, 0, −2 φ, 0}	179	{0, 0, 2 φ, 0}	{0, 0, 0, 1}
79	{0, 0, 0, −1}	{0, −1, −φ, φ²}	188	{0, −1, φ, Φ}	{0, 0, 1, 0}
80	{0, 0, 0, −1}	{0, −φ, −Φ, 1}	199	{0, φ, −φ², 1}	{0, 1, 0, 0}
81	{0, 0, 0, −1}	{−φ², 0, −φ, 1}	212	{−Φ, 0, φ, 1}	{1, 0, 0, 0}
82	{0, 0, 0, 0}	{φ², φ, 1, 0}	38	{Φ, −φ, 1, 0}	{−1, −1, 0, 0}
83	{0, 0, 0, 0}	{φ², 1, 0, φ}	39	{Φ, 1, 0, −φ}	{−1, 0, −1, 0}
84	{0, 0, 0, 0}	{φ², 0, φ, 1}	40	{Φ, 0, −φ, 1}	{−1, 0, 0, −1}
85	{0, 0, 0, 0}	{φ², 0, −φ, −1}	49	{Φ, 0, φ, −1}	{−1, 0, 0, 1}
86	{0, 0, 0, 0}	{φ², −1, 0, −φ}	50	{Φ, −1, 0, φ}	{−1, 0, 1, 0}
87	{0, 0, 0, 0}	{φ², −φ, −1, 0}	51	{Φ, φ, −1, 0}	{−1, 1, 0, 0}
88	{0, 0, 0, 0}	{0, Φ, 1, φ}	52	{0, φ², 1, −φ}	{0, −1, −1, 0}
89	{0, 0, 0, 0}	{0, φ, Φ, 1}	53	{0, −φ, φ², 1}	{0, −1, 0, −1}
90	{0, 0, 0, 0}	{0, φ, φ², −1}	62	{0, −φ, Φ, −1}	{0, −1, 0, 1}
91	{0, 0, 0, 0}	{0, −φ², 1, −φ}	63	{0, −Φ, 1, φ}	{0, −1, 1, 0}
92	{0, 0, 0, 0}	{0, 1, φ, Φ}	64	{0, 1, −φ, φ²}	{0, 0, −1, −1}
93	{0, 0, 0, 0}	{0, 1, −φ, −φ²}	73	{0, 1, φ, −Φ}	{0, 0, −1, 1}
94	$\left\{\frac{1}{2},\frac{1}{2},\frac{1}{2},\frac{1}{2}\right\}$	{−φ, φ, φ, φ}	163	{φ, −φ, −φ, −φ}	$\left\{-\frac{1}{2},-\frac{1}{2},-\frac{1}{2},-\frac{1}{2}\right\}$
95	$\left\{\frac{1}{2},\frac{1}{2},\frac{1}{2},-\frac{1}{2}\right\}$	{−1, φ, 0, Φ}	125	{−1, −φ, 0, φ²}	$\left\{\frac{1}{2},-\frac{1}{2},-\frac{1}{2},-\frac{1}{2}\right\}$
96	$\left\{\frac{1}{2},\frac{1}{2},\frac{1}{2},-\frac{1}{2}\right\}$	{−φ, 0, −1, Φ}	145	{φ, 0, −1, φ²}	$\left\{-\frac{1}{2},\frac{1}{2},-\frac{1}{2},-\frac{1}{2}\right\}$
97	$\left\{\frac{1}{2},\frac{1}{2},\frac{1}{2},-\frac{1}{2}\right\}$	{−φ, −φ², 0, 1}	155	{φ, −Φ, 0, 1}	$\left\{-\frac{1}{2},-\frac{1}{2},\frac{1}{2},-\frac{1}{2}\right\}$
98	$\left\{\frac{1}{2},\frac{1}{2},\frac{1}{2},-\frac{1}{2}\right\}$	{−φ, φ, −φ, φ}	159	{φ, −φ, φ, −φ}	$\left\{-\frac{1}{2},-\frac{1}{2},-\frac{1}{2},\frac{1}{2}\right\}$
99	$\left\{\frac{1}{2},\frac{1}{2},-\frac{1}{2},\frac{1}{2}\right\}$	{−1, Φ, φ, 0}	126	{−1, φ², −φ, 0}	$\left\{\frac{1}{2},-\frac{1}{2},-\frac{1}{2},-\frac{1}{2}\right\}$
100	$\left\{\frac{1}{2},\frac{1}{2},-\frac{1}{2},\frac{1}{2}\right\}$	{−φ, 1, −φ², 0}	146	{φ, 1, −Φ, 0}	$\left\{-\frac{1}{2},\frac{1}{2},-\frac{1}{2},-\frac{1}{2}\right\}$
101	$\left\{\frac{1}{2},\frac{1}{2},-\frac{1}{2},\frac{1}{2}\right\}$	{−φ, φ, φ, −φ}	156	{φ, −φ, −φ, φ}	$\left\{-\frac{1}{2},-\frac{1}{2},\frac{1}{2},-\frac{1}{2}\right\}$
102	$\left\{\frac{1}{2},\frac{1}{2},-\frac{1}{2},\frac{1}{2}\right\}$	{−φ, Φ, 0, −1}	160	{φ, φ², 0, −1}	$\left\{-\frac{1}{2},-\frac{1}{2},-\frac{1}{2},\frac{1}{2}\right\}$
103	$\left\{\frac{1}{2},\frac{1}{2},-\frac{1}{2},-\frac{1}{2}\right\}$	{−1, 1, −1, 1}	103	{−1, 1, −1, 1}	$\left\{\frac{1}{2},\frac{1}{2},-\frac{1}{2},-\frac{1}{2}\right\}$
104	$\left\{\frac{1}{2},\frac{1}{2},-\frac{1}{2},-\frac{1}{2}\right\}$	{−1, φ, 0, φ²}	113	{−1, −φ, 0, Φ}	$\left\{\frac{1}{2},-\frac{1}{2},\frac{1}{2},-\frac{1}{2}\right\}$
105	$\left\{\frac{1}{2},\frac{1}{2},-\frac{1}{2},-\frac{1}{2}\right\}$	{−1, Φ, −φ, 0}	119	{−1, φ², φ, 0}	$\left\{\frac{1}{2},-\frac{1}{2},-\frac{1}{2},\frac{1}{2}\right\}$
106	$\left\{\frac{1}{2},\frac{1}{2},-\frac{1}{2},-\frac{1}{2}\right\}$	{−φ, 0, −1, φ²}	133	{φ, 0, −1, Φ}	$\left\{-\frac{1}{2},\frac{1}{2},\frac{1}{2},-\frac{1}{2}\right\}$
107	$\left\{\frac{1}{2},\frac{1}{2},-\frac{1}{2},-\frac{1}{2}\right\}$	{−φ, 1, −Φ, 0}	139	{φ, 1, −φ², 0}	$\left\{-\frac{1}{2},\frac{1}{2},-\frac{1}{2},\frac{1}{2}\right\}$
108	$\left\{\frac{1}{2},\frac{1}{2},-\frac{1}{2},-\frac{1}{2}\right\}$	{−φ, φ, −φ, −φ}	149	{φ, −φ, φ, φ}	$\left\{-\frac{1}{2},-\frac{1}{2},\frac{1}{2},\frac{1}{2}\right\}$
109	$\left\{\frac{1}{2},-\frac{1}{2},\frac{1}{2},\frac{1}{2}\right\}$	{−1, 0, Φ, φ}	127	{−1, 0, φ², −φ}	$\left\{\frac{1}{2},-\frac{1}{2},-\frac{1}{2},-\frac{1}{2}\right\}$
110	$\left\{\frac{1}{2},-\frac{1}{2},\frac{1}{2},\frac{1}{2}\right\}$	{−φ, −φ, φ, φ}	147	{φ, φ, −φ, −φ}	$\left\{-\frac{1}{2},\frac{1}{2},-\frac{1}{2},-\frac{1}{2}\right\}$
111	$\left\{\frac{1}{2},-\frac{1}{2},\frac{1}{2},\frac{1}{2}\right\}$	{−φ, −1, Φ, 0}	157	{φ, −1, φ², 0}	$\left\{-\frac{1}{2},-\frac{1}{2},\frac{1}{2},-\frac{1}{2}\right\}$
112	$\left\{\frac{1}{2},-\frac{1}{2},\frac{1}{2},\frac{1}{2}\right\}$	{−φ, 0, 1, −φ²}	161	{φ, 0, 1, −Φ}	$\left\{-\frac{1}{2},-\frac{1}{2},-\frac{1}{2},\frac{1}{2}\right\}$
113	$\left\{\frac{1}{2},-\frac{1}{2},\frac{1}{2},-\frac{1}{2}\right\}$	{−1, −φ, 0, Φ}	104	{−1, φ, 0, φ²}	$\left\{\frac{1}{2},\frac{1}{2},-\frac{1}{2},-\frac{1}{2}\right\}$
114	$\left\{\frac{1}{2},-\frac{1}{2},\frac{1}{2},-\frac{1}{2}\right\}$	{−1, −1, 1, 1}	114	{−1, −1, 1, 1}	$\left\{\frac{1}{2},-\frac{1}{2},\frac{1}{2},-\frac{1}{2}\right\}$
115	$\left\{\frac{1}{2},-\frac{1}{2},\frac{1}{2},-\frac{1}{2}\right\}$	{−1, 0, φ², φ}	120	{−1, 0, Φ, −φ}	$\left\{\frac{1}{2},-\frac{1}{2},-\frac{1}{2},\frac{1}{2}\right\}$
116	$\left\{\frac{1}{2},-\frac{1}{2},\frac{1}{2},-\frac{1}{2}\right\}$	{−φ, −Φ, 0, 1}	134	{φ, −φ², 0, 1}	$\left\{-\frac{1}{2},\frac{1}{2},\frac{1}{2},-\frac{1}{2}\right\}$
117	$\left\{\frac{1}{2},-\frac{1}{2},\frac{1}{2},-\frac{1}{2}\right\}$	{−φ, −φ, −φ, φ}	140	{φ, φ, φ, −φ}	$\left\{-\frac{1}{2},\frac{1}{2},-\frac{1}{2},\frac{1}{2}\right\}$
118	$\left\{\frac{1}{2},-\frac{1}{2},\frac{1}{2},-\frac{1}{2}\right\}$	{−φ, −1, φ², 0}	150	{φ, −1, Φ, 0}	$\left\{-\frac{1}{2},-\frac{1}{2},\frac{1}{2},\frac{1}{2}\right\}$
119	$\left\{\frac{1}{2},-\frac{1}{2},-\frac{1}{2},\frac{1}{2}\right\}$	{−1, φ², φ, 0}	105	{−1, Φ, −φ, 0}	$\left\{\frac{1}{2},\frac{1}{2},-\frac{1}{2},-\frac{1}{2}\right\}$
120	$\left\{\frac{1}{2},-\frac{1}{2},-\frac{1}{2},\frac{1}{2}\right\}$	{−1, 0, Φ, −φ}	115	{−1, 0, φ², φ}	$\left\{\frac{1}{2},-\frac{1}{2},\frac{1}{2},-\frac{1}{2}\right\}$
121	$\left\{\frac{1}{2},-\frac{1}{2},-\frac{1}{2},\frac{1}{2}\right\}$	{−1, 1, 1, −1}	121	{−1, 1, 1, −1}	$\left\{\frac{1}{2},-\frac{1}{2},-\frac{1}{2},\frac{1}{2}\right\}$
122	$\left\{\frac{1}{2},-\frac{1}{2},-\frac{1}{2},\frac{1}{2}\right\}$	{−φ, −φ, φ, −φ}	135	{φ, φ, −φ, φ}	$\left\{-\frac{1}{2},\frac{1}{2},\frac{1}{2},-\frac{1}{2}\right\}$
123	$\left\{\frac{1}{2},-\frac{1}{2},-\frac{1}{2},\frac{1}{2}\right\}$	{−φ, φ², 0, −1}	141	{φ, Φ, 0, −1}	$\left\{-\frac{1}{2},\frac{1}{2},-\frac{1}{2},\frac{1}{2}\right\}$
124	$\left\{\frac{1}{2},-\frac{1}{2},-\frac{1}{2},\frac{1}{2}\right\}$	{−φ, 0, 1, −Φ}	151	{φ, 0, 1, −φ²}	$\left\{-\frac{1}{2},-\frac{1}{2},\frac{1}{2},\frac{1}{2}\right\}$
125	$\left\{\frac{1}{2},-\frac{1}{2},-\frac{1}{2},-\frac{1}{2}\right\}$	{−1, −φ, 0, φ²}	95	{−1, φ, 0, Φ}	$\left\{\frac{1}{2},\frac{1}{2},\frac{1}{2},-\frac{1}{2}\right\}$
126	$\left\{\frac{1}{2},-\frac{1}{2},-\frac{1}{2},-\frac{1}{2}\right\}$	{−1, φ², −φ, 0}	99	{−1, Φ, φ, 0}	$\left\{\frac{1}{2},\frac{1}{2},-\frac{1}{2},\frac{1}{2}\right\}$
127	$\left\{\frac{1}{2},-\frac{1}{2},-\frac{1}{2},-\frac{1}{2}\right\}$	{−1, 0, φ², −φ}	109	{−1, 0, Φ, φ}	$\left\{\frac{1}{2},-\frac{1}{2},\frac{1}{2},\frac{1}{2}\right\}$
128	$\left\{\frac{1}{2},-\frac{1}{2},-\frac{1}{2},-\frac{1}{2}\right\}$	{−φ, −φ, −φ, −φ}	129	{φ, φ, φ, φ}	$\left\{-\frac{1}{2},\frac{1}{2},\frac{1}{2},\frac{1}{2}\right\}$

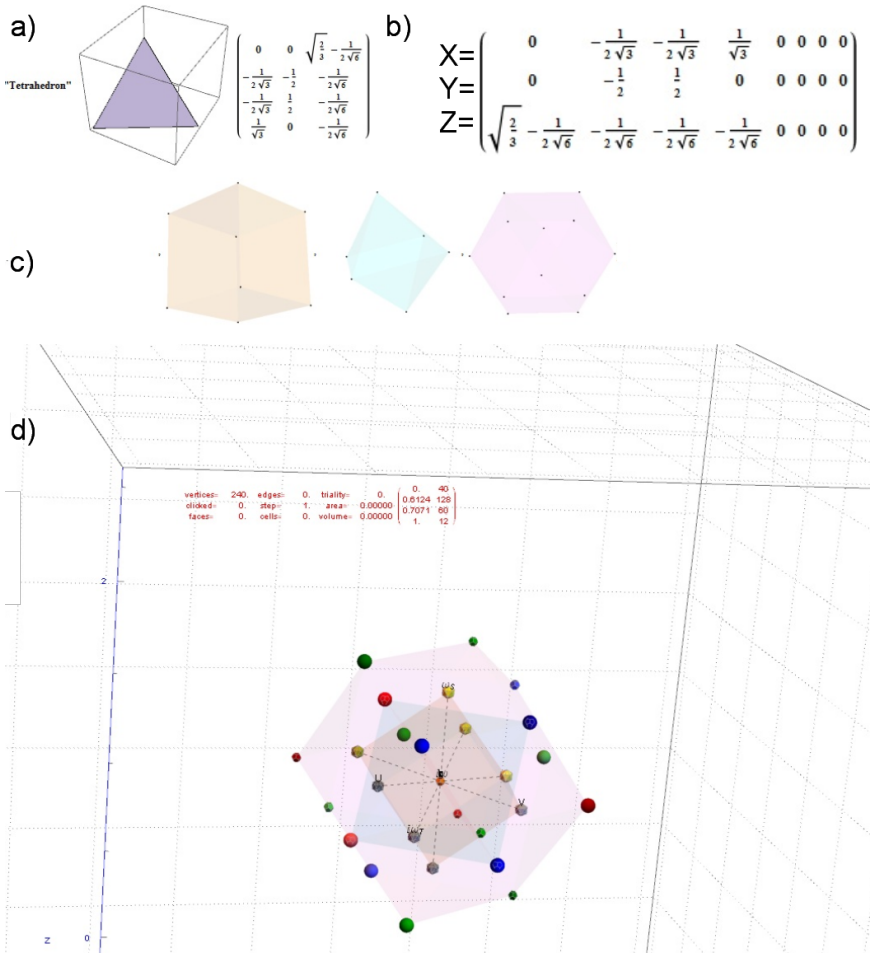

FIG. 13: Tetrahedron Crystal Projection Prism projecting E_8 a) the crystal prism geometry and vertices, b) the selected basis vectors, c) the individual 3D projected concentric hull objects, d) the combined set of concentric objects with progressively increasing transparency and tally of vertex norms

APPENDIX B: HULL PRISM FIGURES

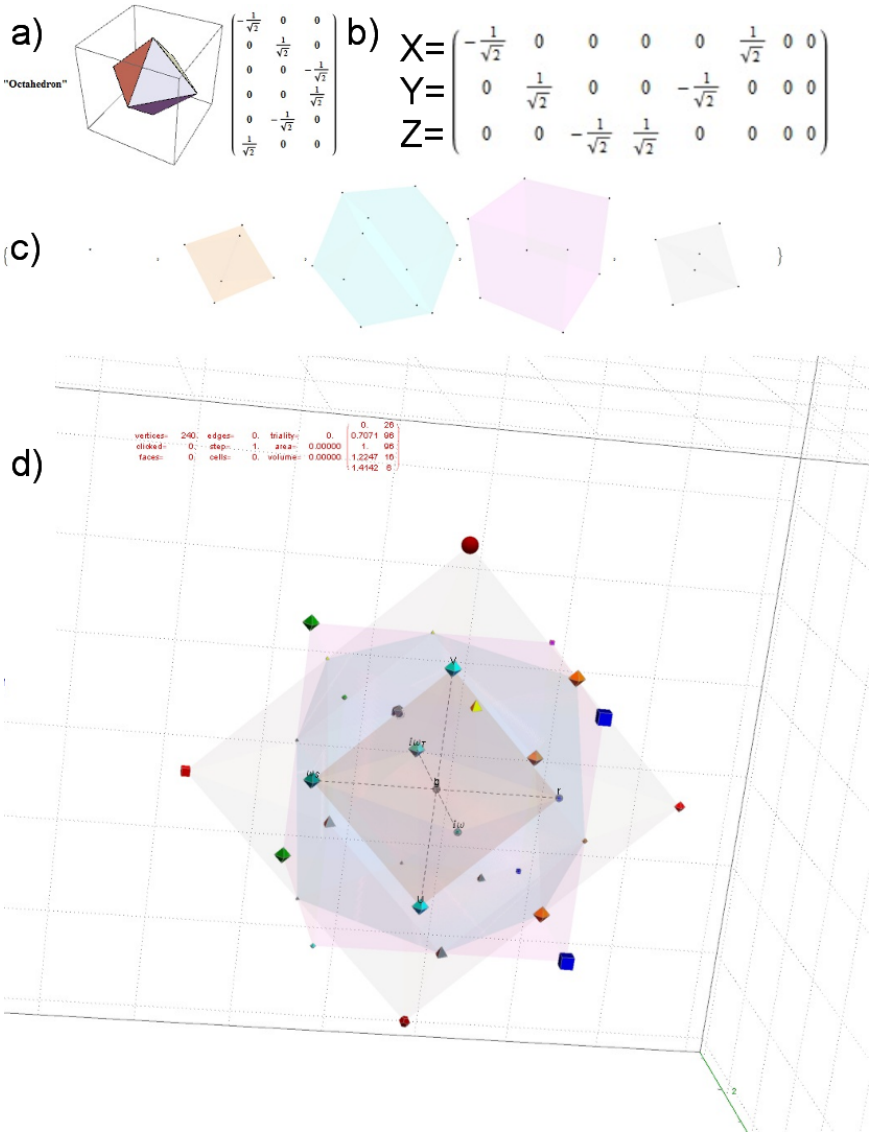

FIG. 14: Octahedron Crystal Projection Prism projecting E_8 a) the crystal prism geometry and vertices, b) the selected basis vectors, c) the individual 3D projected concentric hull objects, d) the combined set of concentric objects with progressively increasing transparency and tally of vertex norms (Note: The Cube also produces the same concentric hull structure scaled by $\sqrt{2}$)

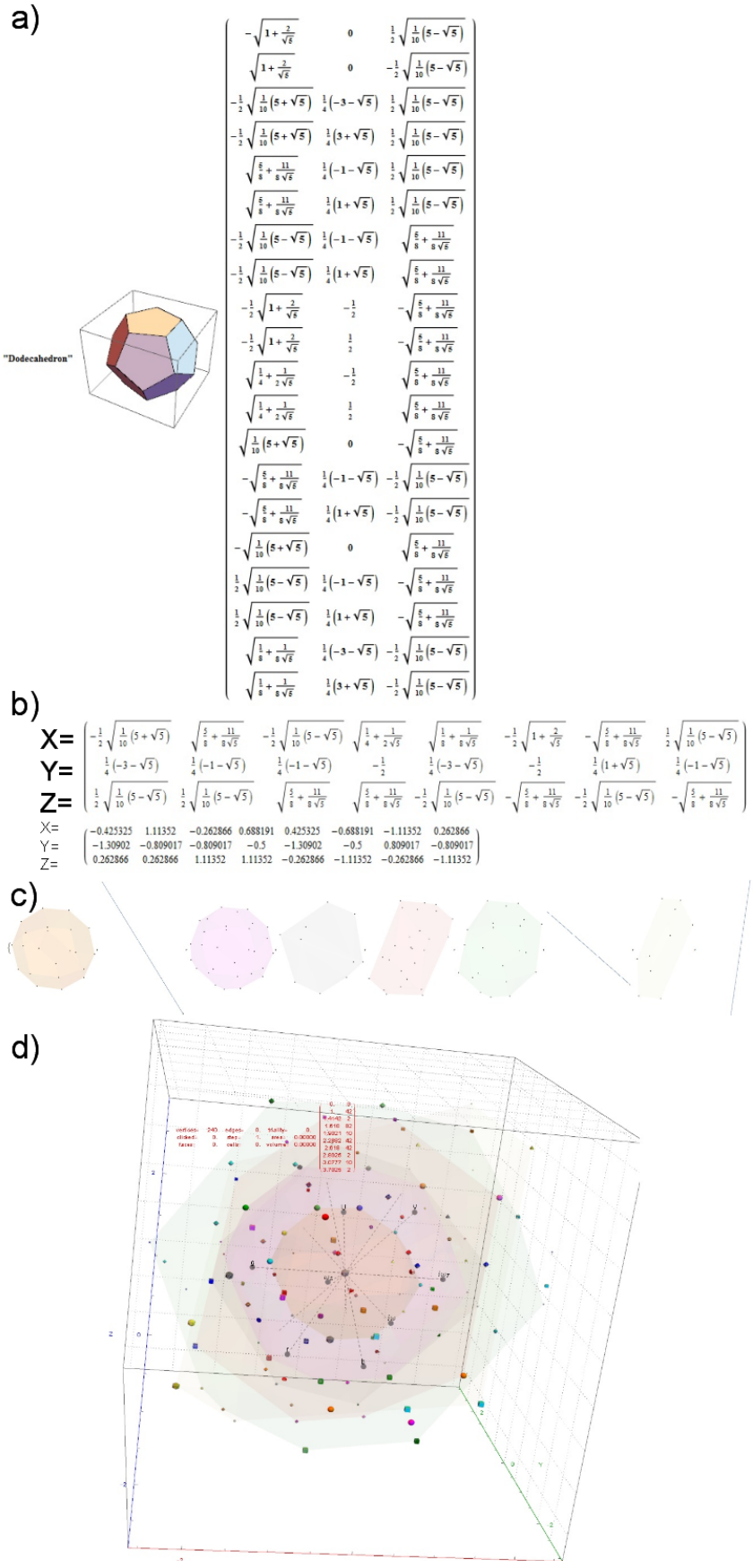

FIG. 15: Dodecahedron Crystal Projection Prism projecting E_8 a) the crystal prism geometry and vertices, b) the selected basis vectors, c) the individual 3D projected concentric hull objects, d) the combined set of concentric objects with progressively increasing transparency and tally of vertex norms

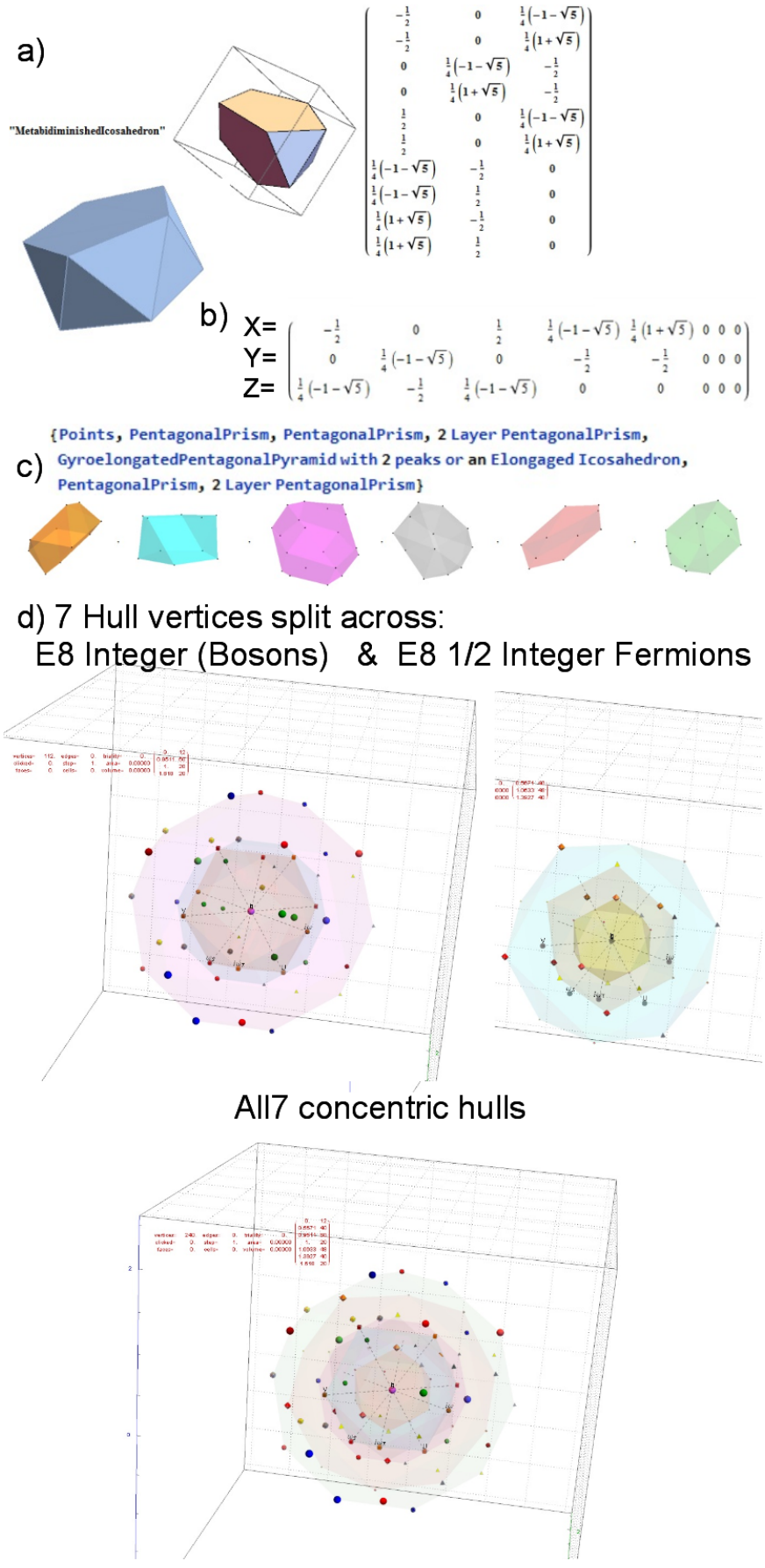

FIG. 16: MetabidiminishedIcosahedron (with its negated vertices gives the GyroelongatedPentagonalPyramid) Crystal Projection Prism projecting E_8 a) the crystal prism geometry and vertices, b) the selected basis vectors, c) the individual 3D projected concentric hull objects, d) the combined set of concentric objects with progressively increasing transparency and tally of vertex norms

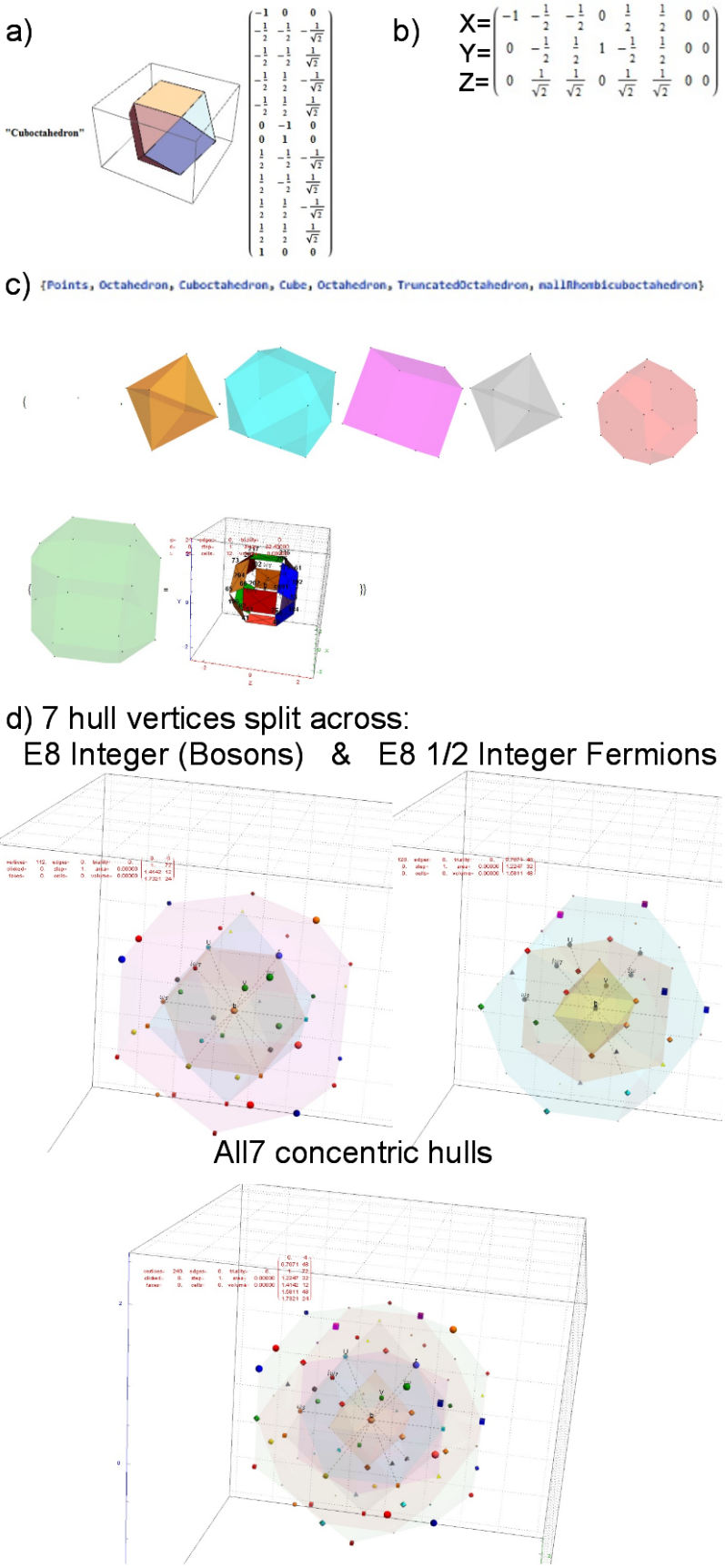

FIG. 17: Cuboctahedron Crystal Projection Prism projecting E_8 a) the crystal prism geometry and vertices, b) the selected basis vectors, c) the individual 3D projected concentric hull objects, d) the combined set of concentric objects with progressively increasing transparency and tally of vertex norms

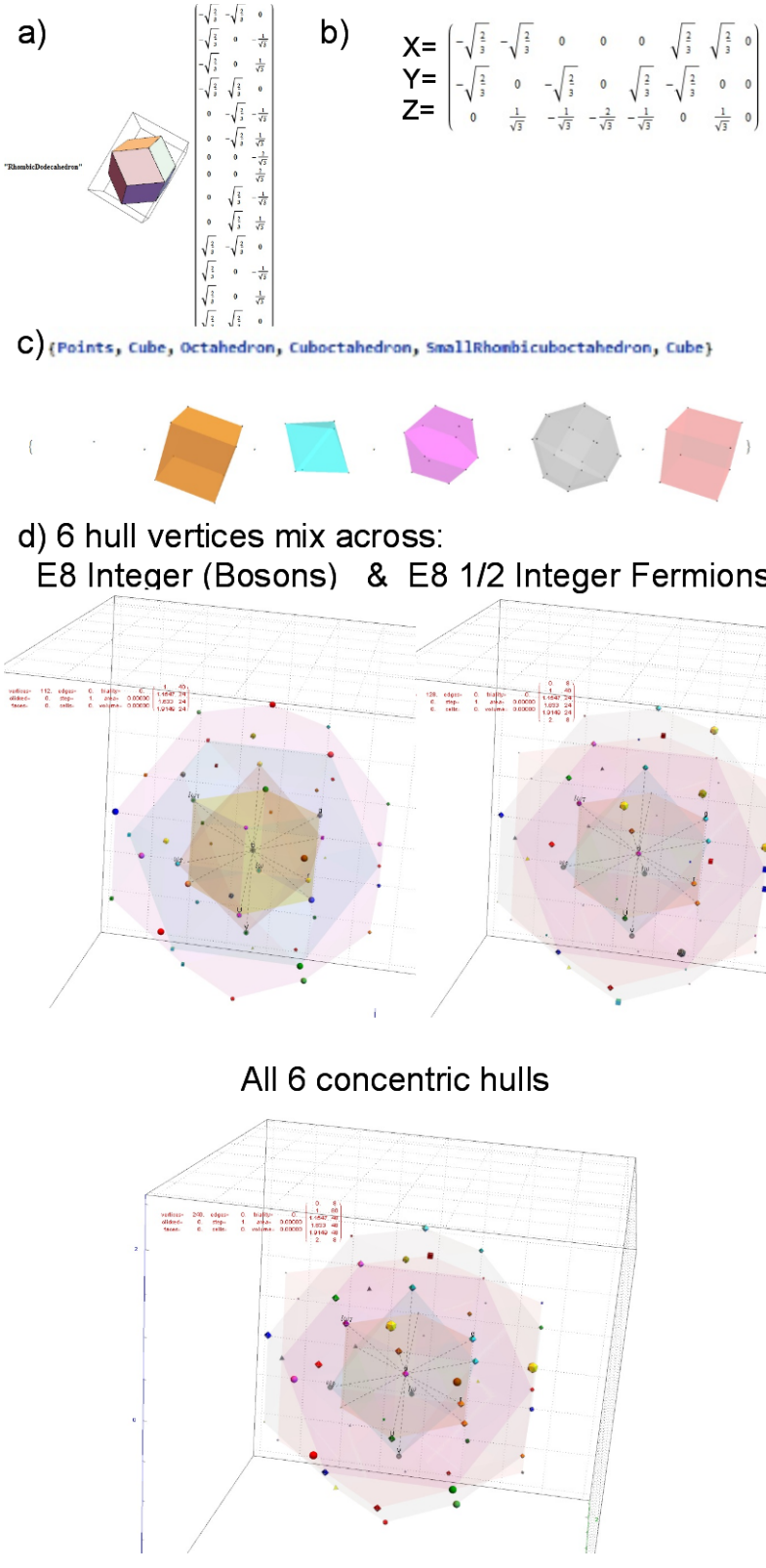

FIG. 18: RhombicDodecahedron Crystal Projection Prism projecting E_8 a) the crystal prism geometry and vertices, b) the selected basis vectors, c) the individual 3D projected concentric hull objects, d) the combined set of concentric objects with progressively increasing transparency and tally of vertex norms